University of Bath

MPHIL

Positron annihilation spectroscopy of voids in silicon

Potter, Nathan

Award date:
2007

Awarding institution:
University of Bath

POSITRON ANNIHILATION SPECTROSCOPY OF VOIDS IN SILICON

NATHAN REES POTTER

A thesis submitted for the degree of Master of Philosophy

University of Bath
Department of Physics
November 2007

Bath, November 2007

_____

NATHAN REES POTTER

Acknowledgements

For providing samples the author would like to thank those at the Universities of Salford, Manchester, Poitiers and Edinburgh, in particular S. Donnelly, V. Visnyakov and M. Beaufort. In addition Universities of Dundee, Southampton and Aberystwyth for providing samples not covered in this thesis. The author would also like to thank R. Mason, D.A. Abdulmalik and the rest of the post-graduate students for help, friendship and support. The author would like to especially thank H. Bone for humour, advice and much needed practical help. Finally the author extends many, many thanks or Prof. P.G. Coleman, for being more understanding and helpful than anyone deserved.

To T.G.

Abstract

An analysis of nanovoided Silicon is presented. The method of production was high dose implantation of Helium ions followed by annealing. This caused production of two species of defect. The first, large voids several micrometers in diameter, are extensively studied elsewhere in literature. The second, previously unknown defect, are shown to be 30-50 atom defects, some of which are decorated with oxygen. A new analysis technique was developed to characterise these defects. It is shown the previously published measurements of the defects are inaccurate and a superposition of clean and decorated defects.

In addition, preliminary work on polarised (magnetised) samples is presented. This utilises the helicity of the polarised positron beam to target spin polarised electrons in iron. It is demonstrated that a clear difference is seen between magnetised and non-magnetised samples even with a weakly polarised beam.

CONTENTS

1. INTRODUCTION

1.1 The positron

The positron, e^+, was the first anti-matter particle postulated or discovered. Predicted by Dirac in 1930 [1], during his work on the electron, it was shown that negative energy (positive charge) particles would also satisfy the electron wave equation. The obvious candidate was the proton, until Weyl [2] observed that the anti-electron must share its mass. Therefore a positron was postulated to have identical mass, but opposite charge to the electron, properties which had not been observed. However in 1932 Anderson [3] noted such a particle during studies of cosmic radiation in a cloud chamber, a particle which followed an electron-like trajectory, but was deflected in the opposite direction (Fig. 1). In a few short years, anti-matter had been both predicted and confirmed but much work would follow, and continue to this day, to understand the positron and its applications in research.

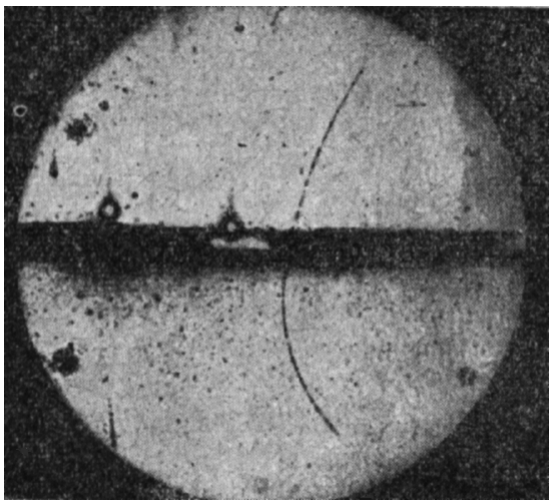

Figure 1 : First experimental image of a positron [3].

The positron can be created in a number of ways. Probably the most common is pair production in a linear electron accelerator. Under CPT (charge-parity-time symmetry) theorem (which the author makes no attempt to explain), high energy photons impacting on a dense nucleus may cause the production of a particle and its corresponding anti-particle [4]. While these may rapidly recombine, if a deviating field is applied to the area of production, such as in Anderson's cloud chamber, the two

particles may move in opposite directions and be distinguished.

Experimentally this is achieved by breaking radiation from accelerated electrons which impinge on a heavy metallic target. The resulting positrons may then be moderated by injection and subsequent re-emission from a suitable material e.g. annealed tungsten. The moderated positions have energy equivalent to the work function of the moderator and may then be accelerated to any desired energy. The primary advantage of such systems is the current, albeit pulsed, of positrons produced. A small LINAC operating at 240MeV is capable of producing a 14mA current of positrons, equivalent to a continuous count of $8.75 \times 10^{17}\ s^{-1}$ [5]. Larger LINACs of 4 and 8GeV are now being used to produce even higher pulsed currents [6]. Such systems are limited more by the electron LINAC and simply by the scale required to produce electrons of sufficient energy. As a result they are invariably one tool among many on a LINAC electron beam.

Of more experimental use is the process of beta decay. An atom may produce a positron by conversion of a proton to a neutron via the weak force [7]. Spin is compensated by production of a neutrino along with the photon, and as the subsequent ion is invariably found in an excited state, a photon may also be emitted. Using Sodium-22 as an example;

$$^{22}Na \rightarrow ^{22}Ne^{*} + e^{+} + \nu_{e} \rightarrow ^{22}Ne + \gamma + e^{+} + \nu_{e}$$

The production of the photon (at 1.28MeV) is useful as a timing signal indicating the production of a positron [8]. It is possible to analyse the fate of a positron by the time between production and annihilation as the time a positron exists is determined by the environment in which it exists. Therefore the recombination time may be used as a material probe.

If a positron is left isolated in vacuum, it is postulated to have a life comparable to that of the electron of $>4 \times 10^{23}$ years [9]. However in any electron density, it will recombine with an electron to produce a photon. The lifetime over which this occurs will obviously depend on the electron density, and therefore the probability of finding an

electron [9].

Recombination of positrons and electrons may occur in one of four dominant forms, which are denoted by number of subsequent γ-ray photons produced. While higher order annihilations (i.e. four-γ, five-γ, etc.) are allowed and do occur [1], these are not significant when compared to lower orders (radiation-less to three-γ) [10,11]. Radiation-less and one-γ annihilation require an atom or ion to be involved in the process to provide additional electrons and again are not significant when compared to the two- and three-γ processes. These occur between positrons and free electrons, where the two-process is dominant [10] producing, at rest, two 511keV photons with 180° separation. This allows energy and momentum conservation between the annihilating particles and subsequent radiation.

However in most experimental circumstances the particles will not be at rest and this momentum must be conserved and is expressed in two ways. Firstly a Doppler shift of the annihilation radiation is observed, and secondly the angular correlation between the two γ-photons is shifted. The aim of much positron research, including slow positron spectroscopy of which this report is primarily concerned, is the detection and analysis of these slight changes.

1.1.1 *Positrons in Materials*

In descriptions of positrons penetrating a material, they are generally assumed to reach a set depth dependent on their initial energy upon entering. This is obviously not the case, as inelastic interactions between positrons and the material instead leave distribution of positrons throughout the material. This distribution is given by

$$P(z,E) = \frac{m z^{m-1}}{z_0^{\,m}} \exp\left[-\left(\frac{z}{z_0} \right)^m \right], \quad \text{where } z_0 = \frac{A E^r}{\rho \Gamma\left(1 + \frac{1}{m}\right)}. \tag{1}$$

Values for A, m and r have been found empirically to be A= 4.0μg cm^{-2} keV^{-r}, m=2, and r=1.6 [8]. $P(z,E)$ may be integrated over z to find the average depth, which is usually quoted as the implantation depth and takes the form of a Markovian distribution.

$$\bar{z} = \frac{AE^r}{\rho} \tag{2}$$

The mean implantation depth is thus proportional to $E^{1.6}$ in silicon. This is important in the qualitative ('by inspection') interpretation of the dependence of positron annihilation parameters on incident positron energy.

Following the positron's thermalisation within the material, i.e. a state of thermal equilibrium with the material, whereby all other energy and momentum is lost via non-elastic interactions, it may further diffuse before annihilating. The range of the diffusion is usually minimal compared to the depth of the initial implant, but is important when concentrations of defects are present in the immediate environment of the positron. The diffusion length distribution of the positron is given by

$$L_+ = (D_+\tau)^{0.5} \quad , \tag{3}$$

where D_+ is the diffusion coefficient of the material in question and τ is the free positron lifetime [9]. Typically the diffusion in a bulk material will be of the order of 100nm. The diffusion is a random walk caused by scattering from phonons. The result of this is positrons in a material diffuse and may find trapping sites (e.g. a vacancy defect, or the surface). Positrons thus annihilate over a range of depths and possibly in different electronic environments.

Following diffusion the positron will annihilate an electron, producing the 2-γ emission already discussed. However if a defect in the crystal lattice exists it is likely that a positron that diffuses into the defects will become trapped due to the lower energy of the defect compared to the surrounding lattice. The local electron environment is then different to that in the bulk, as defects will isolate the positron from high momentum electrons (such as core electrons of the atoms in the lattice) and tend to cause annihilation with either conduction electrons within the defect, or with low momentum (valence) electrons of the atoms surrounding the defect.

1.1.2 *Positron re-emission from solid surfaces*

There is the possibility that an injected positron may, either by diffusion, or by inelastic collision prior to thermalisation, return to the surface of a material [9]. There is in this case the chance of re-emission from the surface, either as (a) a positron or (b) positronium. In order for (a) to occur, the positron work function (the difference between the repulsive dipole potential and the attractive correlation potential) of the surface has to be negative. For (b) to occur at low temperatures, the binding energy of ground state positronium (6.8 eV) has to be larger than the sum of the electron and positron work functions. Epithermal (non-thermalised with some remnant of their implantation energy) positrons returning to a surface are highly likely to escape as fast (~ eV) positrons or as energetic positronium due to their inherent momentum.

The escape of thermalised positrons can be very desirable, as all will have energy equal to that of the work function. Therefore this phenomenon may be used to moderate a beam of positrons to a single energy. As an example, a short experimental study of positron re-emission follows.

1.1.2.1 Measurement of positron re-emission from silicon carbide

The positron re-emission characteristics of a sample of sintered SiC obtained from Rossendorf Research Centre, Dresden, were measured; the sample had been specifically processed for efficient re-emission by annealing the sample to hopefully produce a highly uniform lattice of SiC. Thermalised positrons which have diffused to the surface of the sample without annihilation are then free to leave the sample. To measure the re-emission, an electric field was applied in front of the sample to alternately (i) allow all re-emitted positrons to leave the sample region and not be 'seen' by the Ge annihilation detector viewing annihilation events at the sample through a lead slit; and (ii) return the re-emitted positrons to the sample so their annihilation may be detected.

Potentials alternately of +5V and -5V were applied to the sample in a square wave at 5×10^{-4} Hz. Positrons of energies up to 6keV were injected into the sintered sample, and a number of other SiC samples for comparison. The re-emission is defined as the percentage difference between the annihilation counts at opposite field polarities after removal of background.

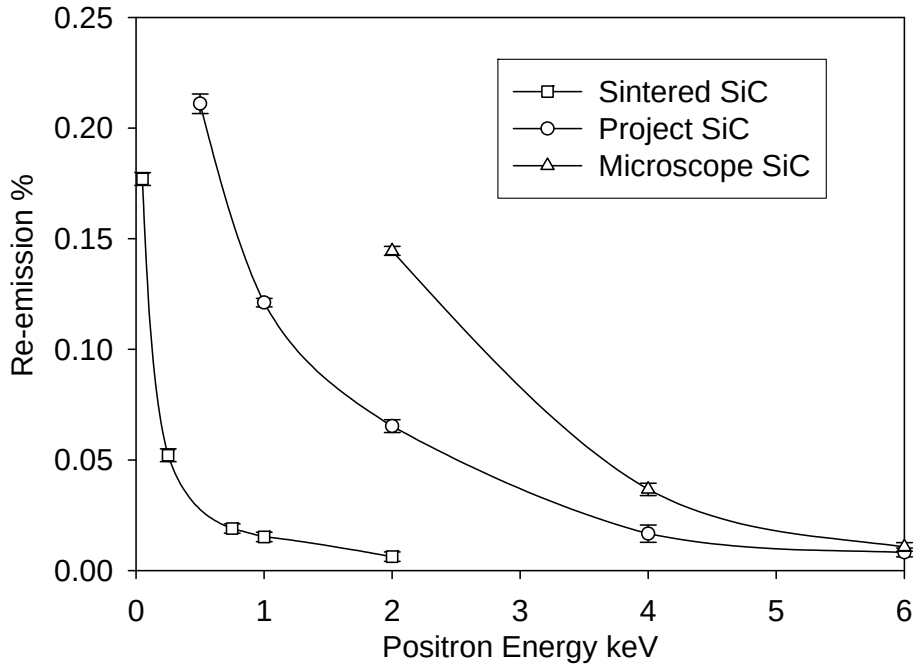

Figure 2 Slow positron re-emission from three samples of SiC as a function of incident positron energy

The Dresden sample gives very low re-emission at high energies compared with alternative pieces of SiC, but exhibits a sharp rise at low (<1keV) injections. This is indicative of epithermal emission, if at rather lower levels than that previously seen [12]. Epithermal emission is likely at the surface as positrons may scatter back to the surface with some remaining implantation energy. There are then less likely to be trapped as this energy will also allow to escape any such defects. The re-emission from pieces of single-crystal SiC used previously in the group's microscope optics and undergraduate projects was found to be much greater, indicating thermalisation followed by work function emission.

By changing the potential to a sawtooth wave of period 2560s, the work-function of each sample may be measured. This was repeated multiple times and the results combined in order to improve experimental accuracy. The results are show in Fig. 3.

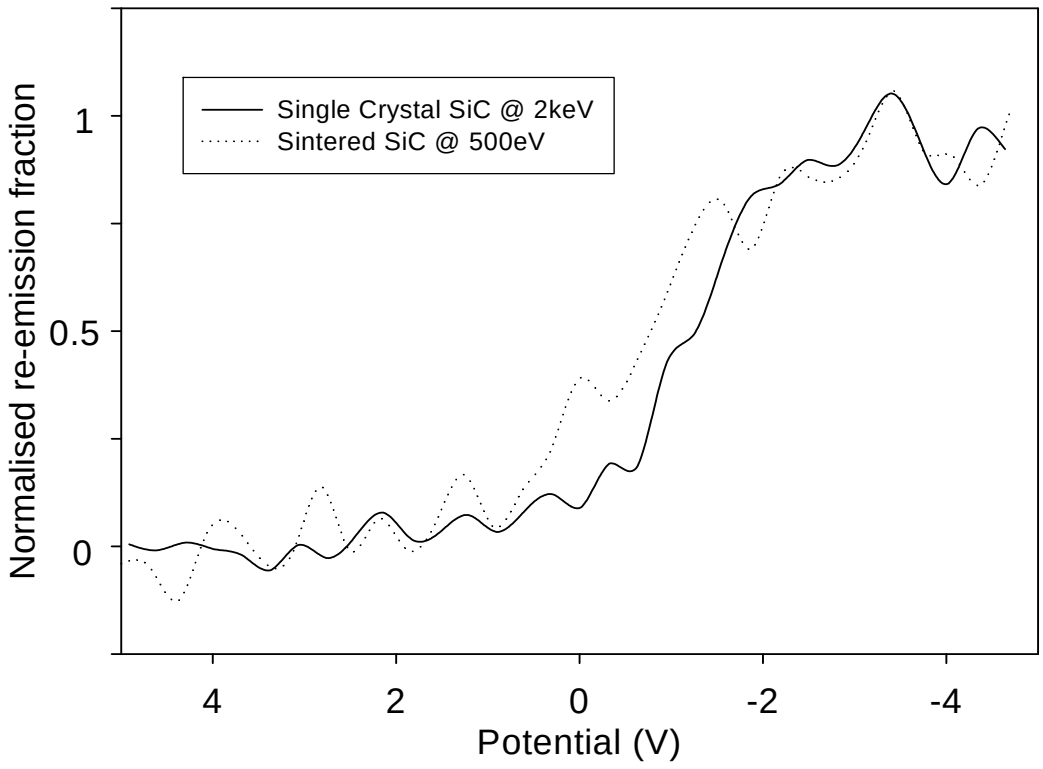

Figure 3 : Positron remission fraction from sintered SiC and single crystal (microscope) SiC. The scales have been normalised to show the same step size and a guide line drawn due to the large number of data points collected.

Injecting positrons at 500eV, it is thought that the ramped response is principally due to epithermal positron emission. The (poorly defined) cut-off at the higher count rate suggests that non-thermalised positrons continue to be emitted from the sample, yet the high energy 'knee' is at the same potential as that of thermalised positron emission from the single-crystal sample. This suggests that there is some poor re-emission from the sample, but the smaller gradient of the step, and the lack of definition of the knee shows that superposition of epithermal emission as well.

Implantation of positrons at 2keV into the sintered sample shows some re-emission, as shown by the gap between the dotted and solid lines around the 0V applied potential in Fig. 3. This reinforces the observations above, because at 2keV epithermal emission is significantly reduced, but some thermalised positron emission may still be seen. Therefore there is some positron re-emission from the sample, but it is insignificant compared with epithermal emission at low energies and negligible at higher.

Comparing a SiC sample with good re-emission at 2keV injection, the sharp knee and steep gradient are contrasted with the sintered SiC. It is interesting to note that firstly there is a small rise at positive potential, which may be due to some weak positron trapping in the sample. This is rapidly superseded by the more prominent thermalised emission, but allows an estimation of the work function as -2.4eV, which is somewhat smaller than previous measurements of ~3eV.

The question is: why is the sintered SiC not a good re-emitter? By examining the Doppler broadening of the annihilation γ for a range of injection energies the structure of the sample may be analysed. Analysis of the *S* parameter vs incident positron energy with VEPFIT models gives a long diffusion length of 162nm. (VEPFIT is the standard Doppler broadening spectroscopy analysis code – see section 1.3.1). By comparison the good emission comes from a piece with a diffusion length of 40nm.

A diffusion length of 162nm is longer than that of most SiC previously studied in our laboratory, and presumably is an effect of the sintering technique employed to produce the sample. It should be expected that a long diffusion length as shown here would lead to a good remission of positrons, although this is obviously not the case. Given the macroscopically rough surface of the material, it is possible that positrons are diffusing back to the surface, but are trapped there and are unable to be escape. The macroscopic roughness is an indication of extreme damage to the crystal structure and as such it is likely that many positron traps (lattice defects) have been formed. These traps Some of the higher energy epithermal positrons can overcome the surface barrier and are detected, as described above.

It may be possible to overcome the surface problems by polishing. However, this may leave a layer of microscopic damage related to the abrasive size and fail to alleviate the problem. There are techniques available to minimise this possibility, which are generally concerned with polishing single crystal SiC, but may be adapted to improve surface of the sintered piece. Generally an undefected surface containing limited potential trapping sites will give the best emission, and thus any technique that helps reduce these defects may also improve emission.

1.1.3 *Polarisation*

Positrons emitted via the positive beta decay of radioactive sources are longitudinally-polarised (i.e., spin-polarised in the direction of their emission) as a consequence of parity non-conservation; the weak interaction that mediates beta decay leads to a non-vanishing helicity [13]. It was discovered in 1979 [13] that the depolarisation resulting from moderation of the beta positrons by a moderator, the basis of the creation of controllable-energy positron beams, is negligible. This opens the door to the possibility of creating highly-polarised beams of mono-energetic positrons to probe non-destructively, and with a degree of depth sensitivity, spin-polarised electrons in thin films or in modified near-surface regions (to depths of a few μm) of materials.

Some pilot measurements on ferromagnetic samples is summarised in section 3.1.

1.1.4 *Positronium*

Positronium, Ps, is a hydrogen-like semi-stable state of interaction between an electron and positron. Proposed in 1934 [14], it is a neutral particle existing in two possible spin states, dependent on where the electron and positron ½ spins are parallel (ortho-positronium) or opposite (para-positronium). Statistically, positronium atoms are found in 3:1, ortho- to para-, ratio [15]. These states eventually decay and annihilate into a number of γ-photons. The conservation of angular momentum of the spins in the positronium gives rise to either odd numbers of emitted photons in ortho-Ps and even numbers in para-Ps. The process is dominated by the three and two γ-processes respectively. The experimental use of this by examining the dominant three γ positronium spectrum and the mainly two γ positron annihilation spectrum the number or ratio of positronium and positron decays may be measured. The lifetime of o-Ps is significantly longer than that of p-Ps, 142ns compared to 125ps [8]. This is due to quantum effects dependent on the number of emitted photons, however a more detailed explanation is beyond the scope of this thesis.

Formation of positronium at the surfaces of solid materials has been a topic of some debate [16,17]. There is evidence that is affected by surface impurities, but it is unknown to what degree these help or hinder positronium formation. What is known is that

positronium must be formed in areas of low free electron density, as high numbers of free electrons will invariably lead to screening of the positron's charge. Thus positronium will not form in the bulk of metals or semiconductors, but can form inside insulators. Near the surface of a metal, however, the electron cloud is sufficiently low-density to allow formation. Therefore it seems likely that surface impurity effects are dependent on the degree of screening they provide. Positronium emission from a solid surface can be stimulated in any material by heating, desorbing positrons bound in the surface state as the energetically-favoured positronium. In this way surface production of thermal-energy positronium is dramatically increased.

Positronium in a material may exchange electron spins with free electrons and convert from o-Ps to p-Ps and vice versa [8]. However due to the short lifetime of p-Ps, it is highly likely that any o-Ps which are converted will decay before being able to change back. Therefore any Ps formed in the bulk of a material will decay as 2-γ p-Ps, both interfering with the annihilation spectra of positrons used in Doppler broadening measurements (see section 1.2 below), and making it more difficult to detect the amount of positronium formed.

It is possible to detect the 2-γ positronium signature using a lifetime measurement on positrons[8]. Using the photon emitted from ^{22}Na beta decay as a start signal, annihilations detected in a component corresponding to a mean lifetime too short to be due to positron decay can be characterised as 125ps p-Ps decay. Therefore a relative measure of positron to positronium decay events can be achieved. Unfortunately systems capable of performing this measurement are not currently available to the author, and thus the fraction of 2-γ bulk positronium can not be calculated in the conventional manner.

1.2 Experimental Methods

Doppler broadened spectroscopy (DBS) is the principal technique used to analyse the samples described in this report. The technique examines the Doppler shift in the energy of the gamma radiation resulting from positron annihilation, which is linked to the momentum of the annihilating electrons, and thus properties of the material in which annihilation occurs [8,9,31]. The distribution of electron momenta is expressed in the observed γ spectrum as a Gaussian-like broadening of the 511keV photopeak (Fig.4). Typically millions of photons would be measured, and peaks would be 10's of keV in width, however exact measurements are dependent on the material, and the key measurement of positron annihilation spectroscopy.

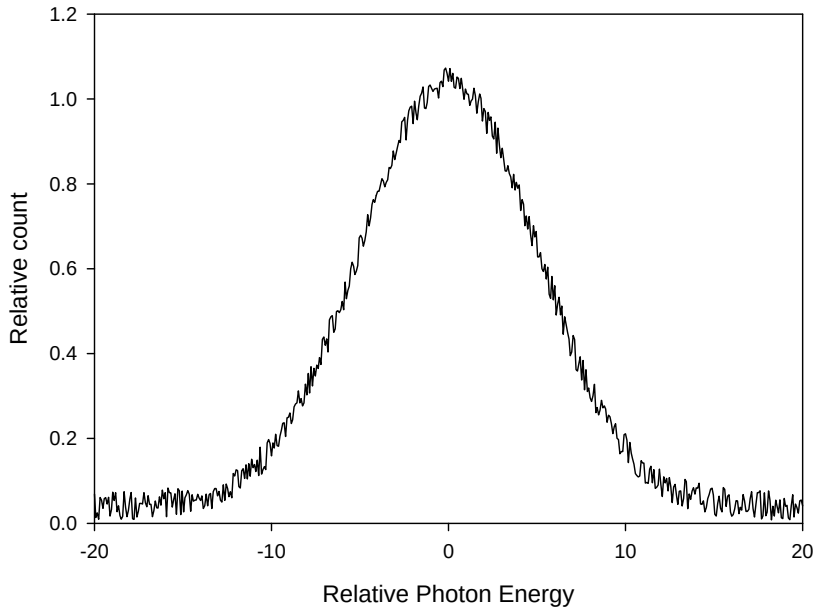

Figure 4 : Gaussian representation of spectral peak. Energy units are arbitrary.

The broadening of the distribution is dependent on the type of electron with which the positron annihilates. If annihilating in bulk material, it is possible that the annihilation will occur with an energetic core electron from a bulk atom. The higher momentum will cause a wider broadening of the spectrum, in comparison to a positron trapped at a vacancy defect where annihilation with a lower-momentum valence or conduction electron is more likely. Generally, the larger the defect, the lower the mean momentum of the annihilating electron, the less pronounced the broadening, and the sharper the peak.

However, such vacancies in the crystal lattice are not only energetically favourable to positron, but any interstitial impurities which may be present in the sample. These may either be unintended, such as Cu in CZ Si, or intentionally implanted. As these will partially occupy preferred positron trapping sites, forming vacancy-impurity complexes, high energy core electrons will become available for annihilations at these sites. Therefore the formation of vacancy-impurity complexes in a sample can lead to broadening of the peak.

All experiments described in this thesis were performed on slow positron beams located at the University of Bath. These are capable of producing a $4mm^2$ beam of positrons at energies between 0.5 and 30keV.

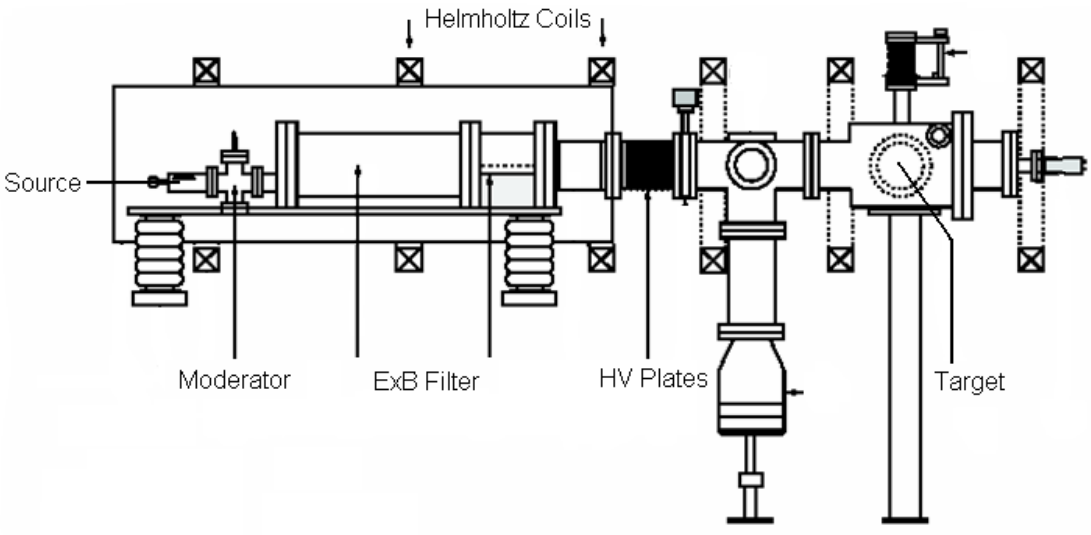

Figure 5 : Diagram of positron beam used at University of Bath.

The purpose of the beam is to produce a controlled, mono-energetic beam of positrons incident on the experimental sample. The positrons are initially produced by a ^{22}Na beta source capsule, in the manner described earlier. These are produced with a range of energies up to 545keV and immediately interact with a moderator, with a small fraction (of the order of 10^{-4}) being re-emitted to form the slow positron beam.

Of the positrons which diffuse to the surface of the moderator about one-third are trapped in a surface well, where they are annihilated, one-third leave as fast

positronium, and one-third are usefully re-emitted with an energy close to the positron work function of the surface. The current moderator of annealed tungsten emits ~3eV positrons and has a fast-to-slow positron conversion efficiency of about $3x10^{-4}$.

Earlier moderators had efficiencies of around 10^{-6}, requiring a pulsed LINAC source to produce a sufficient flux of positrons for useful studies to be undertaken [18]. This was followed by discovery of positron emission from magnesium oxide deposited on a metal plate [19]. This allowed efficiencies of 10^{-5}, but limited the geometry of the moderator. The current use of tungsten originated in 1984, and has been found to have many practical advantages in its handling and production [20]. There is also considerable interest in the development of field-assisted moderators, using an external field to manipulate the surface potential of moderators [21]. It is expected that this would produce a large increase in efficiency, possibly as high as a few percent. Work on SiC, a possible field-assisted moderator, was summarised in the previous section.

Following moderation, the positrons are accelerated slightly (to approximately 100eV) in order to aid subsequent manipulation of the beam. To filter out any fast positrons from the source which penetrate the moderator, an **E**x**B** plate is used as a velocity (energy) selector, deflecting positrons in a pre-determined energy range (around 100eV) into the accelerator coils, while removing any fast positrons by deflecting them only slightly, thus allowing them to be annihilated at a barrier plate which is shielded by lead from the detector. Therefore, only the slow positrons re-emitted by the moderator are selected and guided further down the beam line. This results in a beam containing almost 100% moderated, mono-energetic (slow) positrons.

Following this velocity filter, an electric field is used to accelerate the positrons. In the system described here, this is achieved by applying a potential of up to 30kV across a ceramic tube (in the middle of Fig.5) in which a number of metallic rings are mounted to achieve a uniform field and minimise the chance of breakdown.

The positrons are confined in a magnetic field generated by a number of quasi-Helmholtz coils generating an axial field, co-centric with the flight path of the positrons. This field will introduce helical motion about the central path in any positron attempting to leave it (i.e., with non-zero transverse momentum). This field is

important to both containment of the positron beam, and the size of the beam at the target. The beam spot size is related directly to the diameter of the helical path in the applied magnetic field.

The annihilation photons are detected using a solid state germanium detector with a high energy resolution for gamma ray detection. Typically a million detections may be made for good statistical accuracy, however in some cases short measurements may be taken with maybe ten thousand positron counts. The latter case would likely be used for trial measurement, before longer detection times are set for working data. In the so-called photopeak in the annihilation spectrum (as sketched in Fig.6 below) annihilation photons (of energy 511keV) are absorbed in a photoelectric interaction with a single electron in the crystal, which then transfers the 511 keV to the crystal via the creation of a large number (~2.5×10^5) of electron-hole pairs, which are swept to electrodes to produce an electrical signal whose size , as a result of the high number of electrons produced, is linked with high resolution to the 511keV originally absorbed by the crystal. In order to minimise noise, the detector is cooled with liquid nitrogen, and is isolated by insulating both electrically and mechanically; both forms of noise can create large numbers of small pulses in the detector, which in turn degrade its energy resolution.

1.2.1 *Data collection*

As PAS is a statistical collection technique, sample preparation is relatively easy. Whilst care should be taken to maximise the cross section of the beam interacting with the sample, positrons which miss are simply counted as lost and do not contribute to the measured signal. Such samples are fixed to one or two thin taut wires and visually aligned in the beam. Data analysis, which is of much greater importance to us, is discussed below.

1.3 Data analysis

Whilst it is possible to examine the complete spectrum from a germanium detector, in Doppler broadening spectroscopy it is usual to define basic single-value parameters which describe the shape of the peak. The most common of these are known as *S* and *W* parameters, which are defined as the number of γ-photon counts in a pre-defined energy window over the total number of counts in the photopeak. The S parameter is a quantitative measure of the fraction of counts in the centre of the peak, while the *W* parameter measures the fraction of counts in the two wings of the peak (see Fig. 6). The exact windows used to define the *S* and *W* parameters will vary depending on equipment, personal preference and the aim of the experiment. In order to introduce consistency, and allow comparison of results, most measured *S* and *W* values have absolute values of approximately 0.5 and 0.2, respectively, but are usually quoted in relation to a reference material, usually epitaxially grown silicon [8].

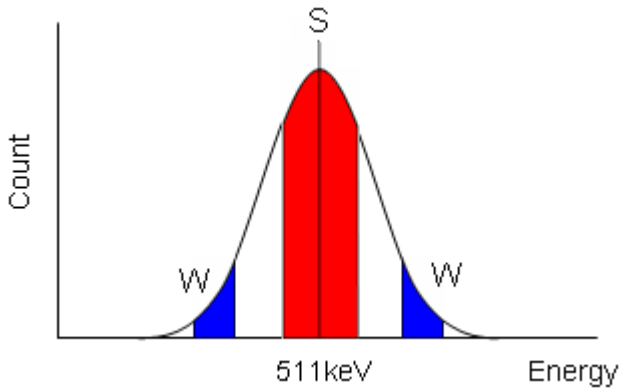

Figure 6 : Schematic representation of S- and W- parameter regions

The magnitude of S (and W) depends on the size of the vacancy defect; using (a) calculations of Hakala et al [22] convoled with experimental energy resolution, and (b) data from positron lifetime measurements, one can propose a defect size dependence such as that in Fig. 7 below. The line of best fit includes both these data sets, and experimental data which provides a maximum possible value for the S-parameter for a sufficiently large defect. The result shows positrons are best suited for examination of small defects below 30 atoms in size, but will detect much larger defects.

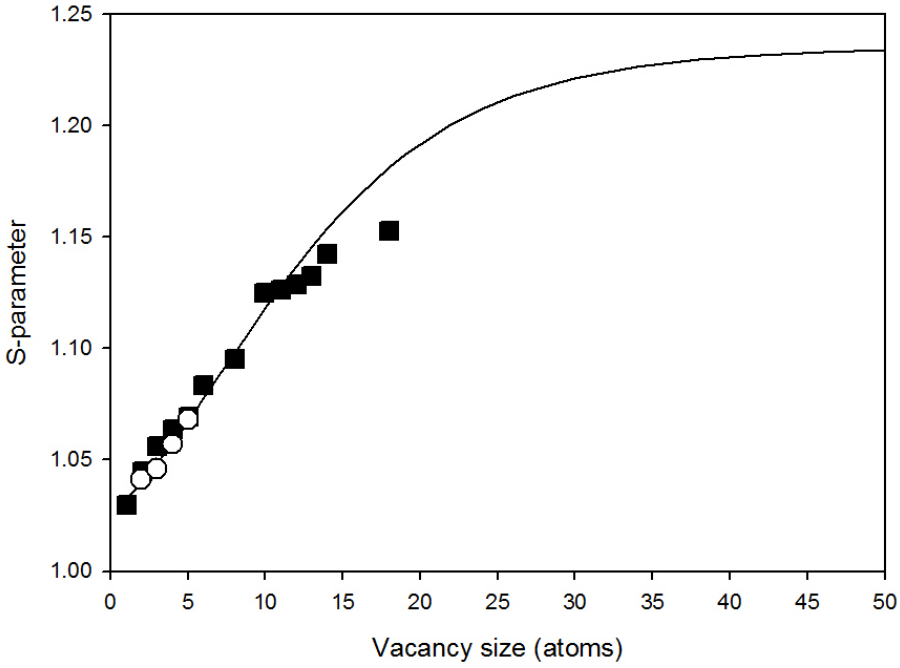

Fig. 7: Comparisons between positron annihilation lifetime spectroscopy and S-parameter measurements of a small number of known defect sizes in silicon. Solid square points are transformed from lifetime measurements [34], open circles are convoluted calculations [22]

An important property of the Doppler-broadened peak is its representation by a linear combination of contributing components. If a number of different annihilation processes can occur within a sample at a given positron implantation energy, the spectrum seen will be a linear superposition of the different processes. This is both a strength and weakness of the technique, and can be demonstrated by considering a hypothetical sample with a buried layer (Fig. 8).

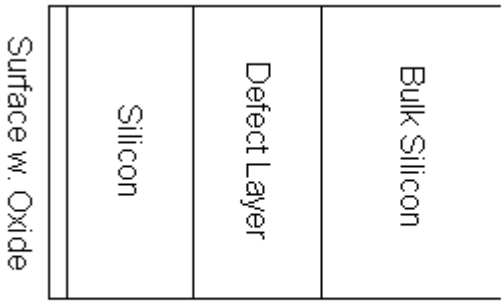

Figure 8 : Structure of a hypothetical sample.

The buried layer contains undecorated voids (of size, say, 4 atoms) in FZ Si; the sample has an oxidised external surface. A plot of *S* against positron implantation energy shows the expected increase of *S* in the void layer. While the *S* parameter of V_4 (a four-atom vacancy cluster) is well known, the positron implantation profile discussed above will mean that the *S* parameter measured is a superposition of the surface state (highly oxygen contaminated), the undecorated voids and the bulk silicon. However, plots of *S* against *W* parameters will "point" towards the three different types of annihilation.

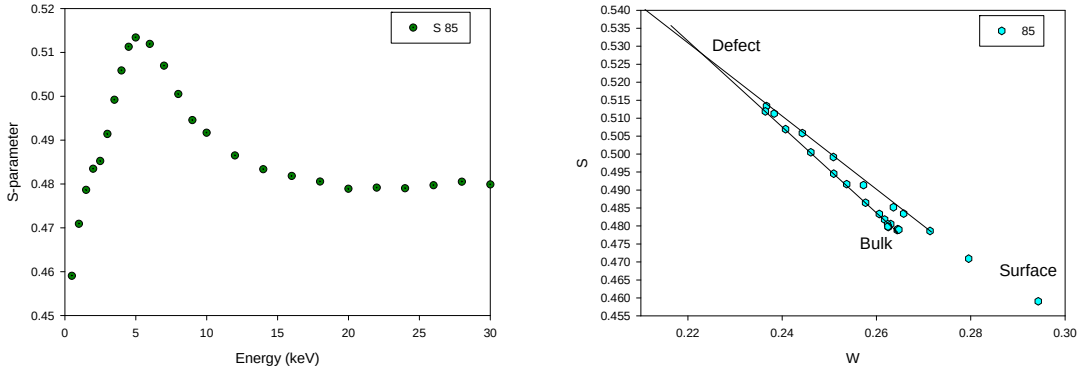

Figure 9 : S-parameter against energy and S-Parameter against W-Parameter for buried defects

Therefore it is possible to evaluate the *S* and *W* parameters for the external oxidised surface, bulk silicon, and the defected layer from extrapolated vertices on the *S*-*W* plot. This is the graphical equivalent of VEPFIT analysis (see 1.3.1 below). Unfortunately the layer *S* and *W* can only be used to determine defect concentration in the layer if

only one type of defect is dominant within a layer. If, for example, the voids in the above sample are partially filled with an impurity ion, the *S* parameter is reduced, as would be expected, but the *S*-*W* plot will now point towards a superposition of empty and decorated V_4 defects. It becomes impossible to distinguish between the two different types of defect, and indeed whether there are two defects at all. The data could also support a single type of defect within the layer, the *S*-parameter of which is below that of undecorated V_4 defects. This is obviously a potential problem of high importance to the classification of material, and an issue that will be returned to later in this report.

As implied in the above example, data interpretation relies on the linearity of *S* and *W* parameters, such that if multiple annihilation regimes exist, with *S* parameters S_1, S_2,… S_N and annihilation fractions f_1, f_2, f_N, a measured *S* parameter, *S*, will be of the form;

$$S = \sum_{x=1}^{N} S_x f_x \ . \tag{4}$$

This allows unknown *S* parameters and fractions to be fitted; however it may also lead to the problem shown above whereby two overlapping annihilation regimes cannot be distinguished from a single combined regime.

1.3.1 *VEPFIT*

VEPFIT is a positron fitting tool written by van Veen et al [32] and is widely used to determine the *S* parameter of layers within a sample from experimental data. The program combines the linearity of the *S* parameter, positron implantation profile and positron diffusion with a fitting routine to estimate unknown parameters. Commonly this would be used to devolve the fraction of positrons annihilating at discretised layers in a sample, and then fit an *S* parameter to each layer, such that the superposition summed to give the experimentally observed value. While it is most commonly used to determine the *S* parameter of layers, VEPFIT may also be employed to fit any linear parameter measured, such as the *W* parameter or annihilation fraction per layer.

The key drawback of VEPFIT is its limitation of only allowing a single defect or

annihilation type per layer in a simple box model. While non-saturated layers of single defects may be overcome by VEPFIT or by the use of an *S*-*W* plot, as described above, the “best fit” for layers of multiple defects will always be a combination of these. This is illustrated in the work described below.

2. STUDIES OF VOIDS

2.1 Introduction

The author will now present a discussion on nano-voided silicon. Positrons are seen to be ideal measures of open volume defects in silicon due to the high trapping potential and subsequent preferential sampling. It was hoped that this sensitivity could then be extended to larger cavities. In order to better describe the voids, a new method of analysis which directly measures the annihilation lineshape was developed.

2.1.1 *Formation of voids*

Porous materials as described in this thesis are normally crystalline materials which have undergone chemical or physical processing to produce voids and bubbles within the bulk of the material. Specifically here we are concerned with semiconductors, most commonly silicon, which have a subsurface layer of voids.

There have been several reasons for the development of such materials. At a very basic level, large interconnecting voids could be used to modify the resistive, capacitative and optical properties of material [23]. Furthermore, as voids are seen as preferential gettering sites for implanted ions [24], there is hope that voids in device materials would allow improved placing of impurities during semiconductor manufacture, and their removal from structures in which they could have deleterious effects. Finally there have also been unexpected commercial processes developed during research on porous materials, the most exciting case being SMART-CUT [25], in which a 2D layer of voids is created which allows the separation of a thin surface layer from its substrate, which is then used in the construction of useful layered structures.

There are two main ways to produce materials containing nanovoids. The first is to generate large cavities in a single step; in the second small vacancy clusters are created, which then are combined through several possible processes to produce larger voids. The main difference between the two possible methods is that, invariably, creation of large cavities in one step involves a chemical process [26], whereas small void agglomeration is an implant technique followed by annealing [27].

A key step in both processes is the characterisation of the voids formed. The voids are usually described in two ways; the average size of the voids and the interconnectivity of the voids. Usually highly interconnected systems are a feature of chemical processing of the material and are generally foam like in nature, with thin walls between voids. While these may be useful to study positron diffusion length within voids and positron/void wall interactions, they are not the focus of the work presented in this thesis.

Voids in all of the samples under consideration have been formed by implant of helium into a silicon lattice [27]. The initial implant, if performed at low temperatures, will produce a mix of helium-decorated and un-decorated monovacancies within the silicon. However, at room temperature there is sufficient thermal energy for the mono-vacancies to become mobile as nearby single atoms have sufficient energy to move into voids leaving an adjacent space; 90% or so diffuse to sinks, and about 10% form the energetically favourable divacancy (V_2) [28]. Further increase in temperature leads to Ostwald ripening of the voids, where now mobile voids may combine into larger and more stable systems or escape to the material surface, and an increased mobility of untrapped helium [28]. At medium temperatures (~700K) larger helium/void complexes may be formed as increasingly large voids become mobile. Free helium will be attracted to the voids, and internal pressure will force the voids to expand further [28]. It is possible that given sufficient free helium, pressure within the voids may be high enough to cause fracture along the depth of implantation. This process, which requires a He implant at a dose $>10^{17}$ cm^{-2}, is known commercially as the SMART-CUT process [25,29].

At anneal temperatures above 1000K, the helium/void complexes undergo further conglomeration into larger defects and ~70% of helium is expunged from the sample due to the high mobility of helium at these temperatures. At higher still temperatures, up to 1200K, all remaining helium is removed from the sample, and the cavities appear to stabilise [27].

The type of defect present in the sample is seen as a function implant density of helium in the sample, and therefore is related to both the energy of the helium implant and the fluence. Defects at lower implant concentrations may evolve as bubble, platelets and

extended defects; however, these may be less stable and removed at high temperature anneals along with the helium. However above a critical fluence, large pores are formed under high temperature annealing, possibly due to the stabilising influence of the large number of helium decorated divacancies initially formed [27].

2.2 Experimental results

Implantation of helium into silicon and subsequent annealing is known to produce cavities and, as outlined above, these cavities lose the trapped helium during annealing and initially begin to coalesce through Ostwald ripening at temperatures above 800ºC. There appears to be little work on either the behaviour of low-energy-He implanted samples, or defect evolution as a function of annealing time. Measurements were made, in an attempt to throw light on these questions, on a series of samples provided by Dr. V. Vishnyakov of Salford University.

2.2.1 *Initial results: Salford samples*

It is important to understand the formation and stability of large defects complexes formed by He-implantation of silicon. Presented here are initial attempts to classify nanovoided Silicon samples using positrons.

2.2.1.1 *Defect Evolution and Stability*

Let us first consider the evolution of nanovoid type defects. While the data sets available do not allow for anything like a complete study of the time dependence of void formation, there is still evidence from which to draw tentative conclusions. The most obvious evidence of sample evolution can be found in sample set 86 (86-4, -2, -1). These are 10keV He^+ implanted samples at $5x10^{16}$ ions/cm^2. Following implantation the three samples have been annealed at 900°C for 15 minutes, 2 hours and 4 hours respectively.

In all three samples a layer of defects is formed close to the surface due to the low energy of the He implant. SRIM modelling [30] of the peak ionisation provides an estimation of 108 (10) nm for the He ion range. This allowed all three samples to be

modelled using an unconstrained dual-layer VEPFIT model; the first layer representing the defected near-surface layer and the second the bulk silicon substrate. The fit results are shown in table 1 below.

Sample number	86-1	86-2	86-4
Annealing Time	4 hours	2 hours	15 minutes
S (voided layer)	0.5426	0.5420	0.5555
Layer thickness	106 nm	105 nm	129 nm
Positron diffusion length in void layer	28 nm	25 nm	43 nm

Table 1 : Unconstrained VEPFIT results for 86- samples.

Using an unconstrained model, however, initially proved problematic. Table 1 illustrates the evolution occurring between 15 and 120 minutes of annealing, however the data is somewhat contradictory. Firstly, the decrease in the *S*-parameter would suggest a decrease in the size of the defects. This may be explained by removal of the helium for the sample between 15 and 120 minutes, but a helium ion or complex is likely to suppress the *S*-parameter, rather than increase it. It is also known from published work that the helium would exit the sample very rapidly at annealing temperatures over 800ºC [28] and therefore is unlikely to be influencing the results of measurements on sample 86-4.

Secondly, it would be expected that if defect agglomeration occurs between 15 and 120 minutes, the *S*-parameter would increase (assuming it does not reach the asymptotic *S* value) as the defect size increases. While it is recognised that the defects go through a series of agglomeration steps, and it is likely that the *S*-parameter for each defect configuration would be unique, the large stable voids expected after sufficient annealing would possess the maximum *S*-parameter. It is therefore thought unlikely that there would be a decrease in *S* to a stable value after sufficient annealing.

The change in the *S*-parameter is also at odds with the layer thickness and diffusion length. If it is assumed that over time there are larger defects forming from agglomeration, then it does seem reasonable that the layer thickness would decrease. During the annealing, there is sufficient thermal energy for defect complexes to

migrate, forming larger and less mobile defects as they meet. As there is likely to be migration towards the surface, we would then see deeper and less densely packed regions of defects consumed by those above them as they migrated. This would be consistent with the shrinking of the layer thickness, but again not the decrease in the *S*-parameter as described above.

The diffusion length change may also be questioned. While there is expected to be an increase in void size, if there were no increase in the number of defects the trapping would be expected to decrease, and thus the diffusion length should increase as positrons are less likely to be trapped prior to annihilation in bulk material. This occurs as the cross-section of the defects will decrease as the size of defect complex increases, assuming that the total number of defects present is constant. However, this may be easily explained by an increase in the total number of defects due to the migration and subsequent concentration of the layer. There is an obvious similarity between the results for samples 86-1 and 86-2, suggesting that any defect evolution occurs before the two hour mark and defects are stable up to four hours of annealing. This is again consistent with the evolution of extremely large nanovoids in the silicon after a period of annealing.

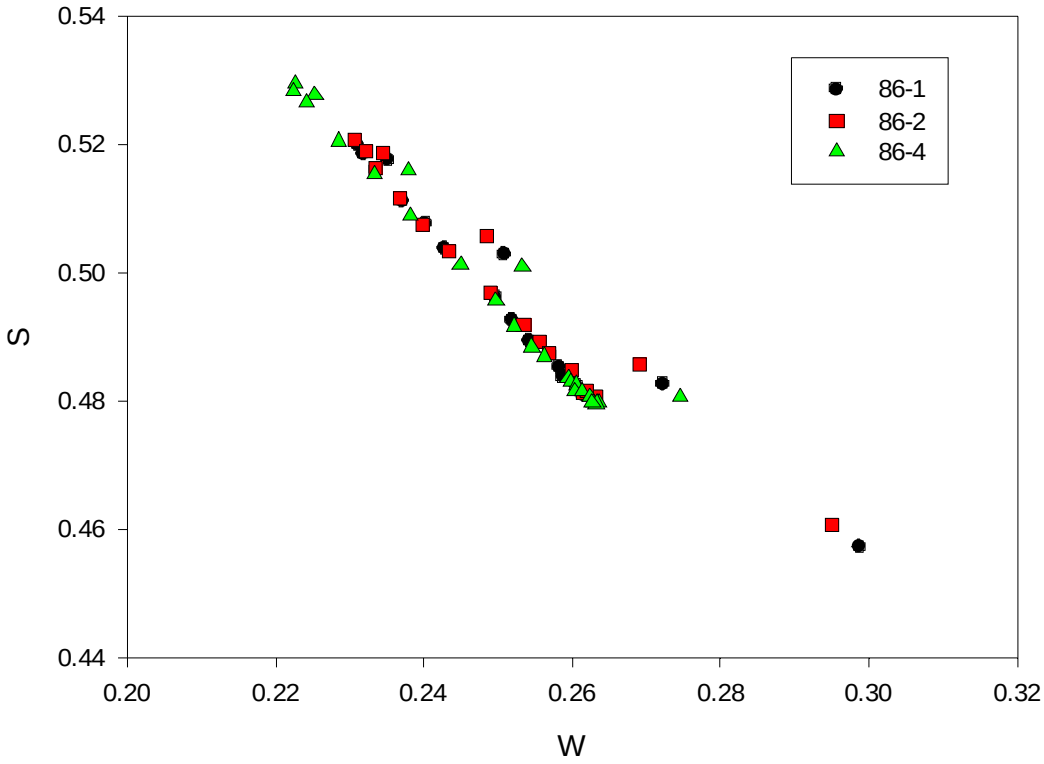

Fig 10. S-W plot of 86- samples.

However, from the literature it is clear that large defects can form in the sample after very short periods of annealing, and nanovoid structures would then exist in all the samples. Examination of the *S-W* plots (Fig. 10) showed that all three samples possessed what appeared to be a single type of defect, with an *S* value which importantly was not located at the asymptotic value. The importance of the second fact will be dealt with in subsequent sections; what is important to this discussion is the existence of a single defect type for all three annealing times.

It was therefore decided to fit the data using an *S*-parameter for the layer of 0.537, as taken from the *S-W* plot measurements discussed above.

Sample number	86-1	86-2	86-4
Annealing Time	4 hours	2 hours	15 minutes
S (voided layer)	0.537 (fixed)	0.537 (fixed)	0.537 (fixed)
Layer thickness	102 nm	105 nm	126 nm
Positron diffusion length in void layer	26.5 nm	24.1 nm	13.9 nm

Table 2 : Improved VEPFIT data for 86- samples.

The VEPFIT model detailed in Table 2. now suggests that if a single defect is responsible for the trapping in the sample, or more accurately, defects with the same *S*-parameter are present in the sample, many of the contradictions seen above may be resolved.

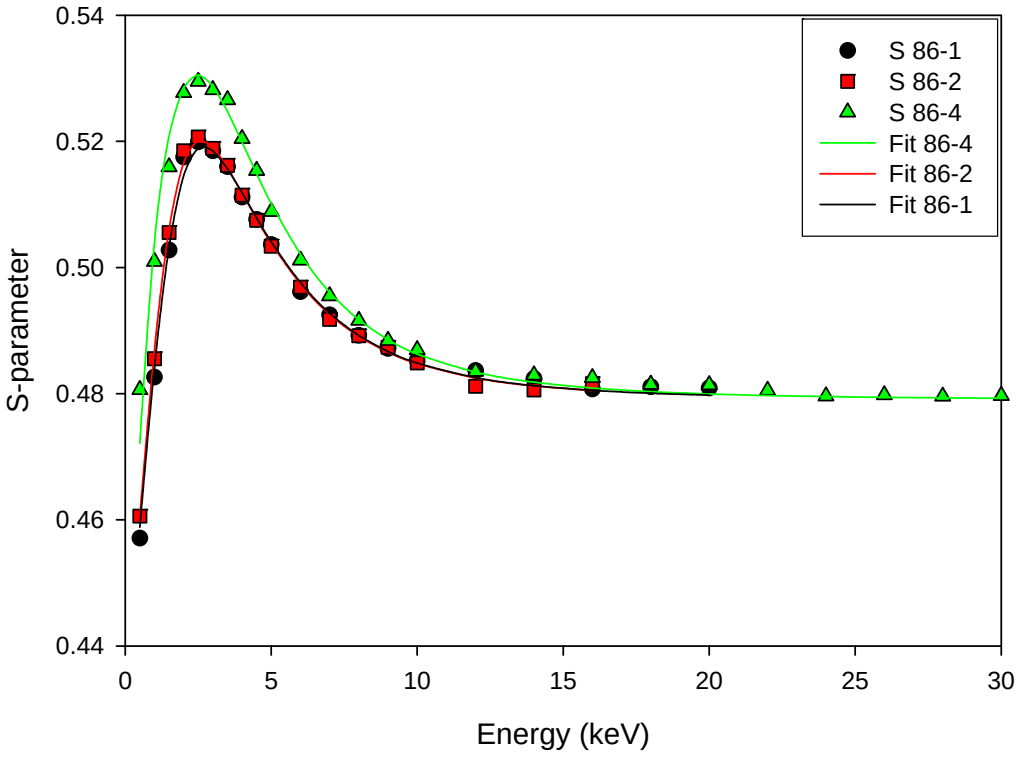

Figure 11 : Experimental (points) and fitted (lines) S-parameters for 86- samples

While the *S*-parameter has been fixed, and such cannot decrease with annealing time as seen above, there is sufficient evidence in literature to assume that some large voids may have already formed by 15 minutes at the 900ºC annealing temperature. While changes still occur in the sample, for example the removal and breakup of smaller voids or continued migration, it is quite possible that even after 15 minutes annealing, the void is the primary source of positron trapping and annihilation.

Unfortunately this is not consistent with the diffusion length calculated from the model. The decrease with annealing time would suggest that the concentration of

defects falls as the sample is annealed, yet the size of the annihilating defect remains constant. This would appear to be consistent with annihilation in smaller defects - if the fitted *S*-parameter is correct, of around 12 atoms in size based on the extrapolation presented in Section 1.3. In this case, there is no evidence of annihilation in large nanovoids, but rather in the formation of ~V_{12} defects. It is possible to use the diffusion length to approximate the number of defects present in each of the samples, using the relationship

$$C = \frac{\lambda}{\nu}\left\{\left(\frac{L_{bulk}}{L_{eff}}\right)^2 - 1\right\}, \tag{5}$$

where ν is specific trapping rate, usually taken to be $5n \times 10^{14}$, where *n* is vacancy size, λ the positron annihilation rate in pure silicon (4.54×10^9 s^{-1}) and *C* is defect concentration per atom.

Sample number	86-1	86-2	86-4
Defects/atom (±10%)	6.7×10^{-5}	8.1×10^{-5}	2.4×10^{-4}
Defects/cm^3 (±10%)	6.1×10^{17}	7.5×10^{17}	2.3×10^{18}

Table 3 : Defect concentrations for 86- samples based on fitted diffusion length

It is thought that samples 86-1 and -2 are identical to within experimental error. However, as the defect concentration is proportional to $(L_{eff})^{-2}$ the difference is obviously magnified. This still leads to a markedly lower concentration of defects in the longer annealed samples, but also shows a possible difference between samples 86-1 and -2. While the lower concentration still leads to saturation in the layer, it also allows more injected positrons to diffuse to and decay in the bulk and at the surface. This develops the lower peak *S* seen in the experimental data of samples 86-1 and -2.

The data from sample set 86 may be compared to sample 89, in which 5×10^{16} He ion/cm2 were implanted at 40keV prior to annealing for 30 minutes at 900ºC. The raw data for this sample are shown in Fig. 11 below.

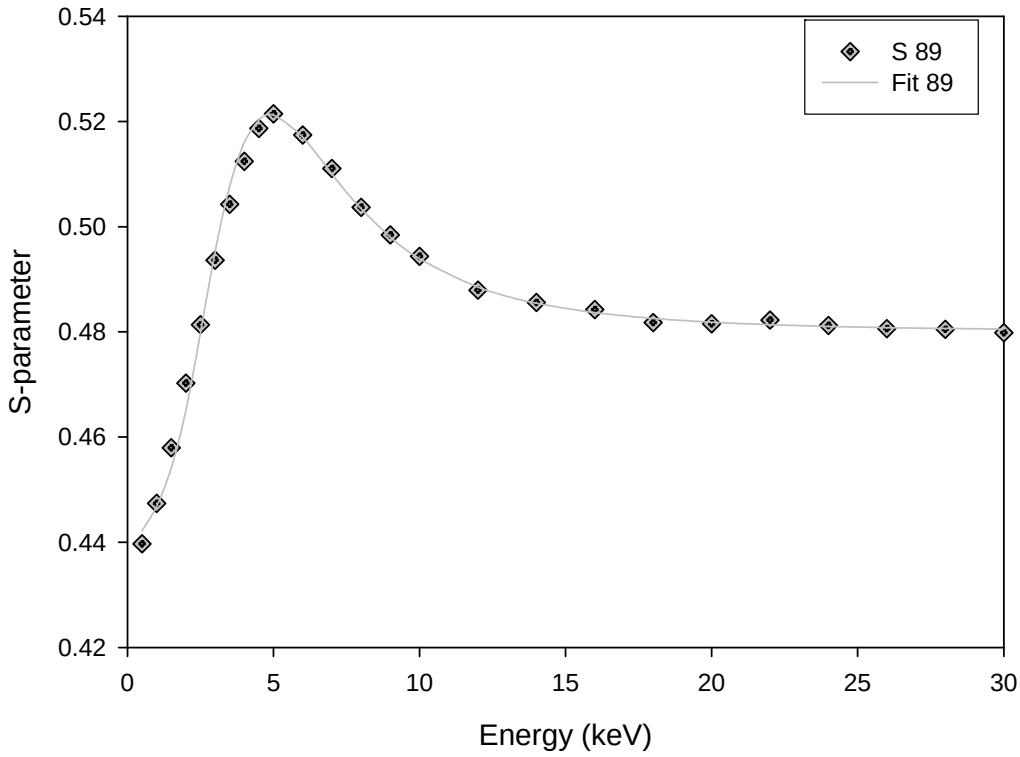

Figure 12.: Measured and fitted S parameters for sample 89.

While there is one obvious difference between this sample and the 86 set, the depth of the implant, the defect evolution was assumed to be similar under annealing. The defect layer would be deeper and wider due to the higher energy of the implant. This may affect the evolution of the layer thickness and concentration somewhat, as defects would no longer be free to move to the surface of the sample and escape. In effect the defect layer would no longer be pinned at one edge by the surface, as seen in the lower energy implant.

The best fit of experimental data was obtained with a three layer model, including a narrow surface layer, again as a result of the higher energy implant. Few He ions were of sufficiently low energy to damage the near-surface silicon, and the slight damage would have been totally annealed out. The surface layer required fixing of diffusion length and S-parameter to avoid VEPFIT fitting of extremely high values. This illustrates another weakness of the VEPFIT code, with tendencies to produce the best fit, with little regard for physical meaning. A good fit was obtained using a fixed *S*-parameter of 0.537 in the defect layer, taken from the 86- dodeca-vacancies and

confirmed using the *S-W* plots for this sample.

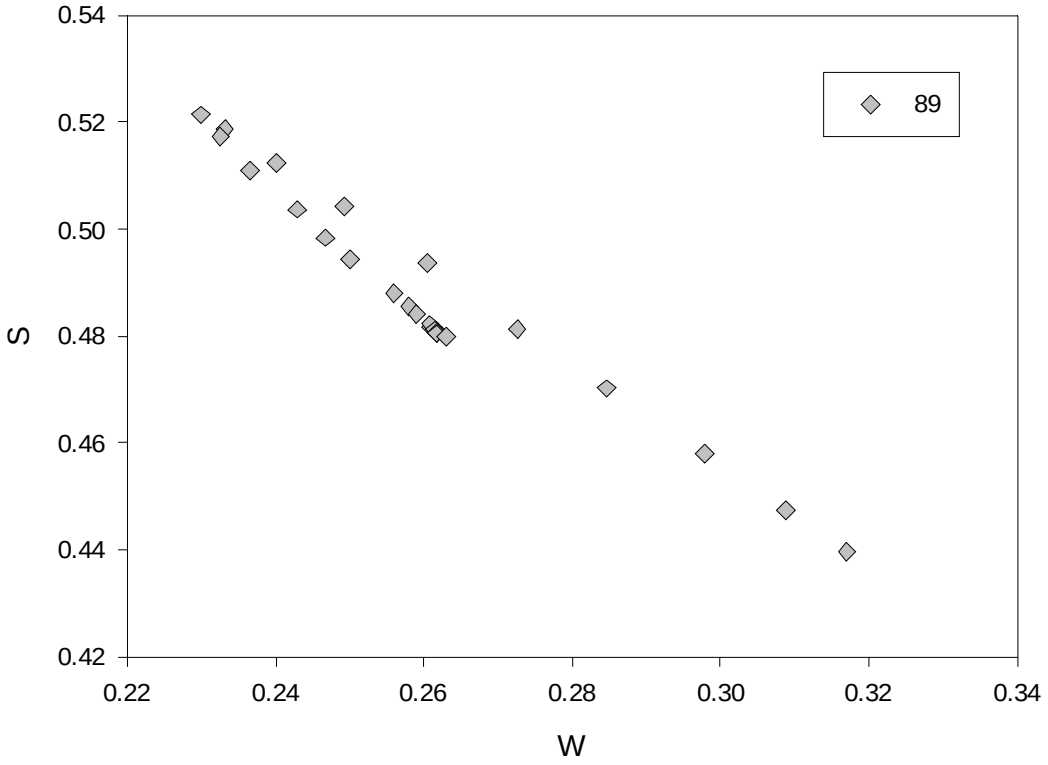

Figure 13 : S-W plot for sample 89.

Sample 89	Layer 1	Layer 2	Layer 3
S-parameter	0.435 (fix)	0.537 (fix)	0.48 (fix)
Length	93nm (fit)	291nm (fit)	n/a
Diffusion length	72 nm (fix)	38nm (fit)	100nm (fix)

Table 3 : VEPFIT parameters for sample 89

It is obviously difficult to make comparisons between the 86 and 89 samples based on the layer thickness and diffusion lengths, due to the difference in implantation energy. However it is assumed that the same type and size of defects will form, and thus it is possible to instead compare their concentrations. It is seen that the concentration decreases after annealing, notionally as defects combine or dissociate, before stabilising somewhere between 15 and 120 minutes. This may be used as a qualitative measure of the stability and evolution of the defects.

Calculating the concentration of the defects in the voided layer gives C = 3.2 x10^{-5}

defects/atom (2.9 x10^{17} defects/cm^3). This is lower than the concentrations calculated for the lower energy samples and would appear to be equivalent to that of a long-anneal sample, but the defects are spread over a greater depth. Comparing 89 and 86, it should be expected that defects are spaced over 2.3-2.8 times the volume and therefore concentration should be an equivalent factor smaller. The normalised concentration is 7.3-8.9 x10^{-5} defects / atom. This shows that the 30-minute anneal almost produces the stable situation, but may still require further annealing to reach such a point.

To summarise, the data indicated that a single size of defect is present in all four samples and appeared likely to be a dodecavacancy. During annealing the defects probably diffuse towards the surface leading to a thinner defected layer and longer positron diffusion length. The concentration of the defects is believed to be the best measure of their evolution, and it can be seen that the defects continue to evolve somewhat after 30 minutes of annealing, and are stable after less than 120 minutes. While it appears that the defects are close to their final state after the 30 minutes, it is impossible from these measurements to deduce unambiguously a minimum time for the equilibrium state to be reached.

2.2.1.2 *Minimum Implantation Concentrations*

There is a minimum or threshold dose for void formation, and therefore it is useful to determine the minimum ion dose for which the voids are detectable by positrons. It is important to stress that this does not necessarily mean the minimum dose that will form voids, but rather the minimum dose that will form sufficient voids to be detected.

For this we will consider two samples; 91A and 92. 91A was implanted with 10keV He at a dose of 1x10^{16} ions/cm^2 before annealing at 700ºC for 30 minutes. Sample 92 was implanted with 10keV He at a dose of 2x10^{16} ions/cm^2, but was not annealed. S-parameter measurements for each sample is shown in Fig 14 and 16 respectively.

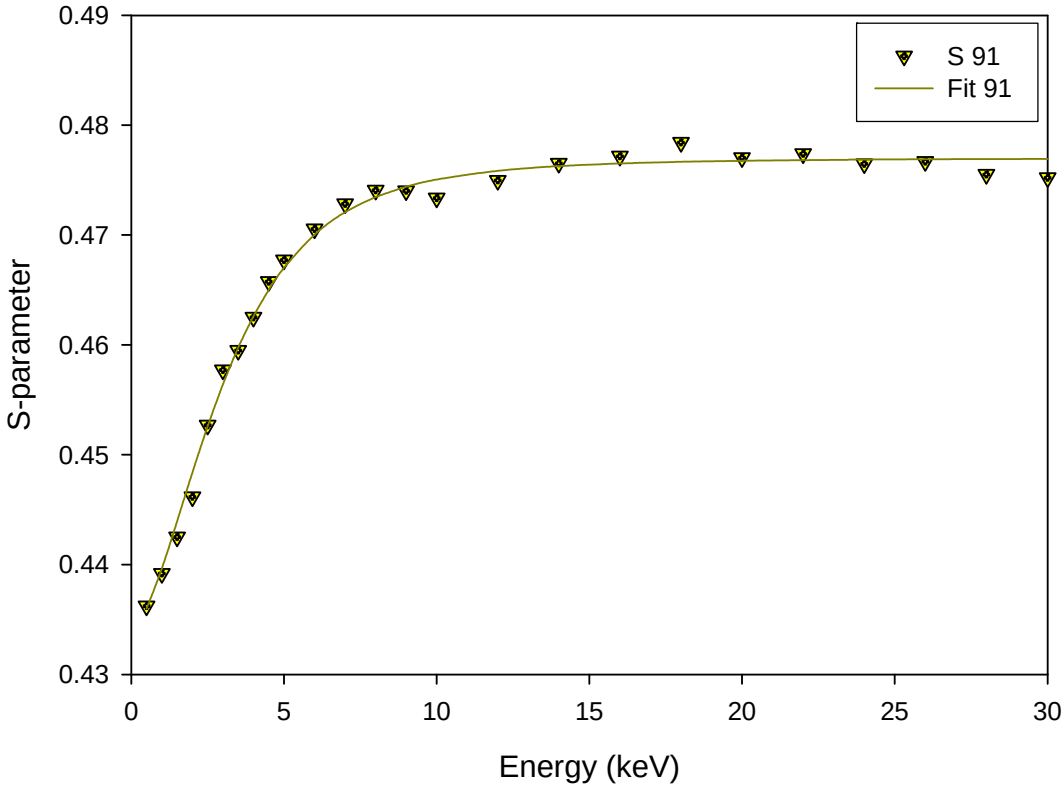

Figure 14 : Un-implanted- like response seen in sample 91A

Sample 91A exhibited a response similar to that of unimplanted Si with an oxide layer at the surface as shown in Fig. 11. This was initially unsurprising, as it appeared that all damage had been annealed out of the sample, due to the low implant dose failing to generate enough stable vacancies. However, 86-1 and 86-2 still showed a response after long anneals, and the literature is ambiguous as to whether the temperature of annealing is sufficient to repair all damage over 30min produced by the low flux of helium. It is therefore more likely that the damage still existed, but was hidden by the oxide layer. An obvious test of this would be etching to remove the oxide and allow the damage to be observed.

Fitting was achieved by an oxide on substrate single layer model, as would be expected to fit an un-implanted sample. This may show that all damage has been annealed under the low dose, or simply that any response is hidden by the oxide layer. This would occur if the defect response was small compared to the gross difference between bulk and surface. The fit does not model the fluctuations at ~10 and 17 keV

which (given the low energy of implantation) are likely to be experimental.

S-Surface	0.434
S-bulk	0.477

Table 4 : Single layer parameters for sample 91A. Box fitting as an oxide on substrate.

Examination of *S-W* plots (Fig. 15.) show the energy points to lie on a single straight line between surface *S* and bulk *S*. This lends further credence to the single layer model described in Table 4, which cannot resolve any void-like defects from the low dose implantation.

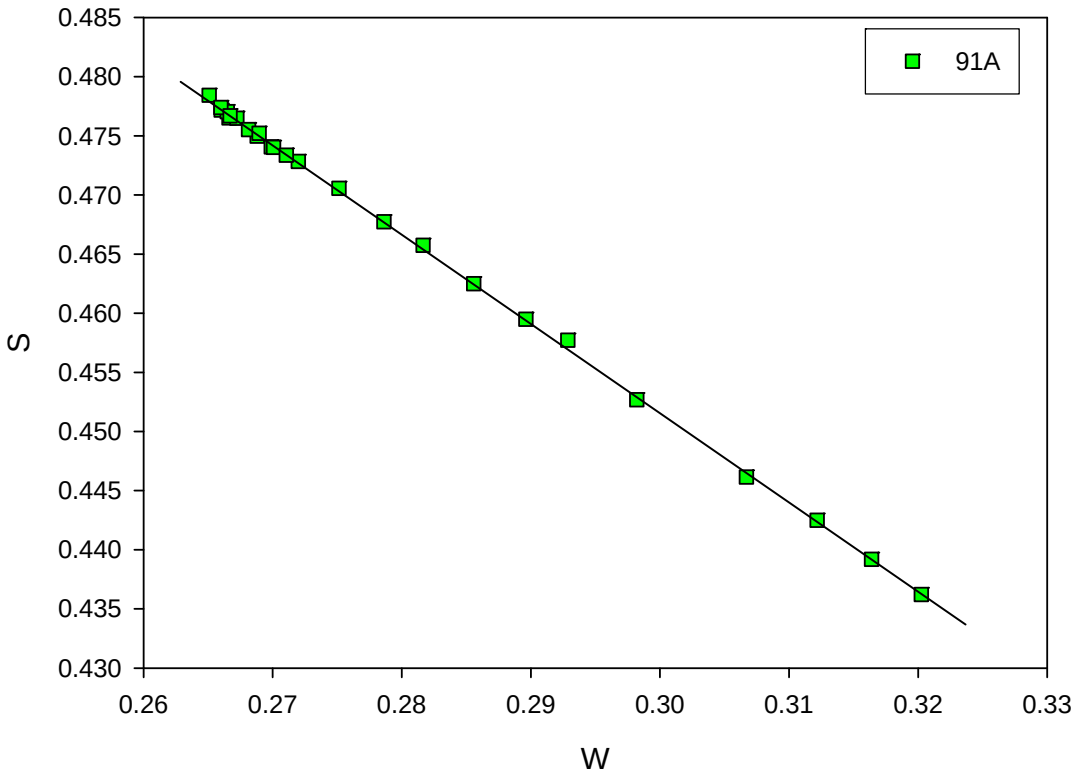

Figure 15 : S-W plot for sample 91A.

Sample 92 had a higher ion dose implanted than 91A, but the damage has not been annealed. The *S* parameter now shows a damage peak, but the implantation dose was not sufficient for the defect response, which is lowered because of He decoration, to overcome the tendency to low oxide values as the positrons diffuse to the external surface. This leads to a flattened region of interest with an obvious defect layer, but no

useful information can be extracted.

The position of the flattened region does correspond to the peak of annealed defects in sample 86. This is illustrated by the comparison in Fig. 16. The distortion of the peak is primarily due to a small defect response, indicative of lower positron trapping rates being overpowered by the shallow positron implantation profile and the surface oxide response. A much clearer result would be seen if surface oxide were removed (eg by HF etching).

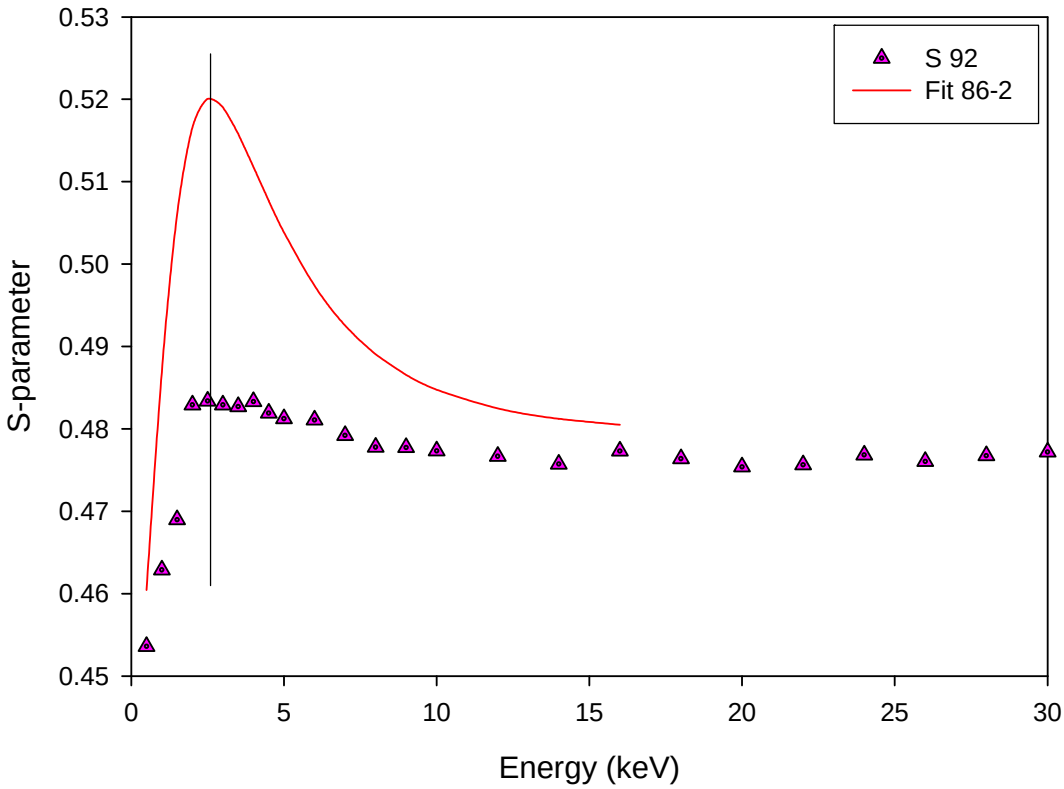

Figure 16 : Comparison of data for samples 92 and 86-2.

The data were difficult to model due to the very steep fall off when approaching the surface. A two layer model provided the best fit, but was still unable to model both the reasonably flat void response and the fall to the oxide value. Further modelling found that a good fit could not be obtained with such a rapid fall off, even with a three layer model.

It is therefore likely that an implant of greater than $2x10^{16}$ ions/cm^2 is required to

produce detectable large defects in silicon. Although detectable damage begins to occur in sample 92, which may have formed defects if annealed, the damage is poorly defined and distorted by the surface oxide response. It is therefore impossible to determine unambiguously the level of defect concentration, and whether such a stable defect layer would form.

2.2.2 *Initial results: Edinburgh samples*

Two sample FZ Si wafers, implanted with 7.0 and 7.25x10^{16} He ions/cm^2, before and after annealing, were provided by Dr J. Terry and Prof. L. Haworth of the University of Edinburgh. Raw *S* parameter data for these samples showed a characteristic bump at low energies similar to that seen for sample 86. These have been fitted using VEPFIT models and defect data obtained from the Salford samples previously discussed.

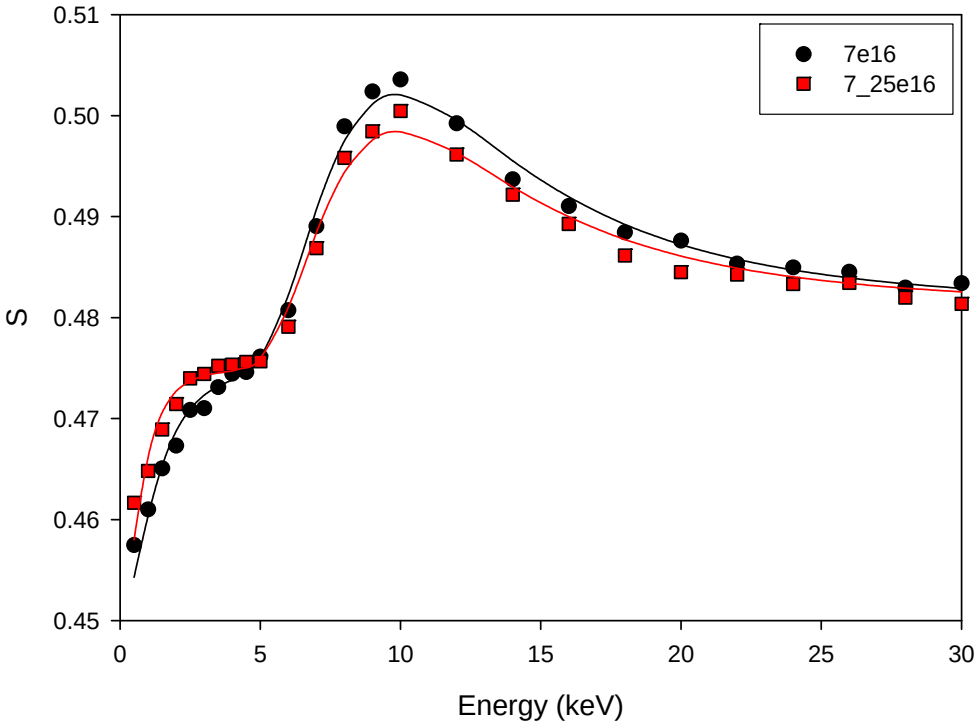

Figure 17 : 150kV He ions in Si with two doses (labelled): after annealing

A three-layer fit was required for both sets of data; a near surface damage region, the main defect peak and the bulk silicon. Corresponding to previous results the peak was found to have a dodecavacancy response, both in its *S*-parameter and layer diffusion length. The near-surface damage was fitted using an *S*-parameter obtained from the *S-W* plot and was found to be below that of bulk silicon. The bulk diffusion length was found to be 250nm, a more acceptable result that the low values seen in all of the other samples. The fitting results for the two samples are summarised in tables 5 and 6 below.

7.0 x 10^{16} cm^{-2} 150keV He in Si

Layer:	Near-surface	Defect	Bulk
S-parameter	0.475 (fixed)	0.537 (fixed)	0.481 (fixed)
Diffusion length	30.6nm (fitted)	25nm (fixed)	250nm (fixed)
Layer thickness	508nm (fitted)	288nm (fitted)	n/a

Table 5 : VEPFIT parameters for sample implanted with 7x$10^{16}$$cm^{-2}$ He (annealed)

7.25 x 10^{16} cm^{-2} 150 kV He in Si

Layer:	Near-surface	Defect	Bulk
S-parameter	0.475 (fixed)	0.537 (fixed)	0.481 (fixed)
Diffusion length	14.5nm (fitted)	25nm (fixed)	250nm (fixed)
Layer thickness	513nm (fitted)	215nm (fitted)	n/a

Table 6 : VEPFIT parameters for sample implanted with 7.25x$10^{16}$$cm^{-2}$ He (annealed)

The data for the un-annealed samples (Fig. 18, below) showed a response to a defect region, with a characteristic *S* value lower than in the equivalent layer after annealing (and thus assumed to be affected by the presence of helium ions). The near-surface damage seen after annealing is not apparent in Fig. 18 and is thus believed to be caused by annealing.

An alternative possibility is the existence of a thin buried oxide layer or oxygen decorated complexes near the surface. It is assumed that the complex will take the form; V_xO_y, where the complexes are form from a vacancy of size x decorated with y atoms of oxygen. Both oxides and decorated complexes would have the effect of lowering the *S* parameter in the defect layer.

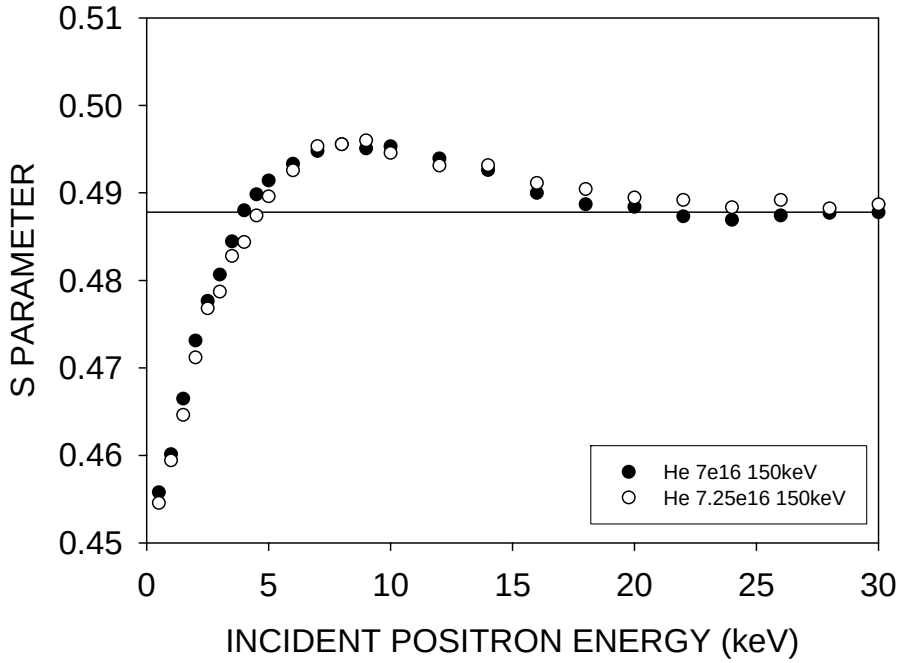

Figure 18 : S-parameter measurements of un-annealed Si samples implanted with 150keV He

It has been only recently that examination of this type of voided silicon has become popular. There has been considerable work with high doses and implantation energies of helium in silicon [27,28,29]. In particular, interest in the Smart-Cut process has fuelled much work in growth of helium bubbles.

However, this work has revealed two important results. The first is the stability of the observed voids throughout annealing. While more critical damage, either from higher ion fluences (greater than two orders of magnitude difference) or deeper implants would be expected to be stable, Ostwald ripening would lead us to expect that damage close to the silicon surface would be annealed away. This is obviously not occurring and would lead us to believe that either that the V_{12} voids formed during the early stages of ripening are either very stable, or there is some kind of pinning in the voids causing them to remain throughout the annealing.

Secondly is the characterisation of the V_{12} voids themselves. Previous work on this type of silicon has produced similar results to those presented above, showing an exact match in normalised *S*-parameter, and similar values for layer thicknesses and positron

diffusion lengths [17]. The characterisation was made from an extrapolation of S-parameters found for smaller silicon vacancies. Further, running VEPFIT simulations of positrons in porous silicon reproduced the experimental data with a good degree of accuracy.

However characterisation of the V_{12} voids is dependent on them being the only defect caused by the helium-vacancy evolution, despite the fact it was known that large bubbles (comprising of $>10^3$ atomic vacancies) must exist in the material through previously published results and TEM analysis of similar samples to those analysed.

2.3 Gaussian Analysis

As discussed earlier, the DBS technique uses the energy of the annihilation photon as a measure of the momentum of the annihilating electron. Positrons enter a material at a controlled energy, but rapidly thermalise, possibly being trapped in a defect, before annihilating with an electron. The result is two photons, with approximately 180º separation. If annihilation occurred with both electron and positron at rest, the energy of each photon would be 511keV. However as the electron momentum must be conserved the photon energy is perturbed from the at-rest value. Statistically averaging this change in energy over many annihilation events results in an energy distribution broadening out from 511keV. This Doppler-broadened spectrum is characteristic of the material environment and such may be examined to yield useful information.

Traditionally DBS is most useful where only a limited number of annihilation sites are present in a material. While different annihilation regions may be resolved under favourable circumstances, it is also possible that overlapping defect sites are wrongly classified as some combination of the two.

However, the time-averaged annihilation spectrum of a single defect can be approximated to a Gaussian of width characteristic to that defect. Therefore, by superposition, multiple annihilation sites may be represented by multiple Gaussian curves, the amplitude and width of each corresponding to the annihilation fraction and S-parameter.

2.3.1 Method of Analysis

The implantation profile of positrons into a material follows a Makhovian distribution (Eq. (1)), and it is likely that spectra for all positron implantation energies will show annihilation at surface and bulk sites. It is therefore initially important to characterise the Gaussian curves of surface and bulk states. Fitting implantation energies of 0.5keV to 2keV and 24keV to 30keV of bulk silicon with surface oxidation allows fitting of these components. The width of these may be checked against fitted *S*-parameters of these regions for further confirmation by constructing regions of interest and calculating the appropriate ratio. In cases where damage or defects do not allow a

single Gaussian to these regions, a library value may be used instead, preferably one measured recently to minimise the effect of experimental drift in laboratory equipment.

The aim of these fittings is to reduce the number of unknown annihilation sites and therefore fitted Gaussians in regions away from the bulk and surface. Ideally these would only contain a single type of defect, along with convolved surface and bulk fractions, which can easily be fitted using VEPFIT and other tools as mentioned above. However, in the case of multiple defect types, simple fitting may incorrectly fit S_{fit} where S_{fit} may in reality be $S_{fit} = S_{d1}f_{d1} + S_{d2}f_{d2}$, where d1 and d2 are different defect types.

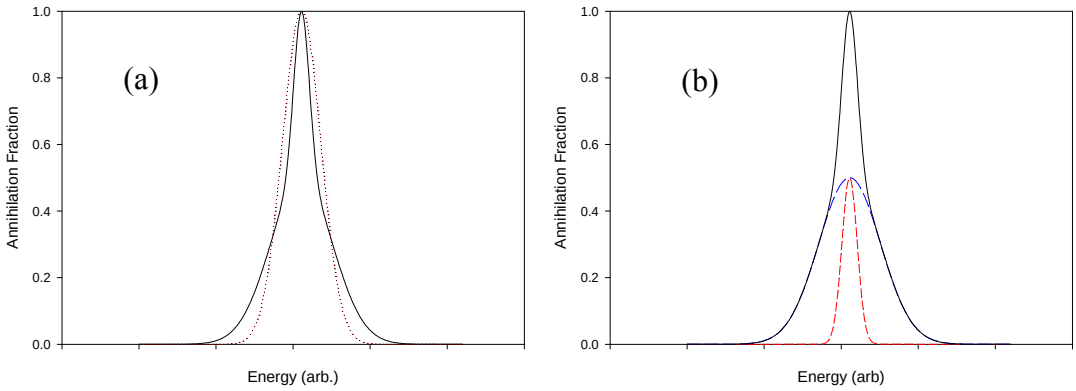

Figure19: (a) Example of simulated S-parameter (solid) and attempted fitting with single Gaussian (dotted): (b) Two Gaussians (long dash and short dash).

Consider a region containing two defect types; one with a large *S* of, say, 1.2 and another with an annihilation peak corresponding to an *S* of 1.05 in a 1:1 ratio. It is assumed that the bulk (conventionally normalised to an *S* of 1.0) and surface is removed from consideration for this example. It is also assumed that once the positron has encountered a defect, it is trapped until annihilation. In such a case the measured S-parameter will be the superposition of the two traps, 1.125, and may be fitted assuming a single combined defect type. Unfortunately fitting with the single defect does not represent the actual system described, as demonstrated in Figure 19 (a).

However, the *S* parameter is in fact a fairly crude method of characterisation, ignoring

the finer detail seen in the actual annihilation peak. Therefore attempts to fit with a single Gaussian of width 1.125 will not reflect this detail and such a solution will be discounted. Fitting with multiple Gaussian curves will fit the finer detail and such a two Gaussian model (of widths 1.2 and 1.05) seen in Figure 19(b) will both better fit the superimposed data and correctly represent the system.

From the fitted Gaussian curves both the S-parameter (by constructing regions of interest) and the annihilation fraction in each defect (from the relative height of each Gaussian) may be obtained. This may be checked against the measured *S* parameter to confirm the fit.

2.4 Gaussian analysis of nano-voids

Gaussian analysis has been used to analyse a number of samples, in particular those with helium-created bubbles. Extensive measurement was performed on sample P1 (from Poitiers) which was known, through electron microscopy, to have a layer of large bubbles caused by agglomeration of helium-formed bubbles (Fig. 20). The scanning method is reported in Ref. 23, and was conducted on this sample by collaborators at Poitier.

Analysis of *S-W* parameters using techniques already detailed found similar voids to that of the Salford sample set. The voids are V_{10} defects, the slightly smaller size may be due to the higher implant temperature (400°C compared with room temperature for Salford samples). This would have increased the initial freedom of movement of the implanted helium, allowing stable agglomerations to form more readily. Otherwise the sample appeared similar in terms of defect layer depth and thickness to the Salford set. SRIM calculation again confirmed that the peak of the V_{10} defects is at the same depth as the peak damage caused by the helium implantation. While this does again not rule out the possibility that the bubbles appear as V_{10} defects, the measured size of the bubbles (0~20nm) mean they are likely to appear as clean internal silicon surfaces, with a response similar to bulk.

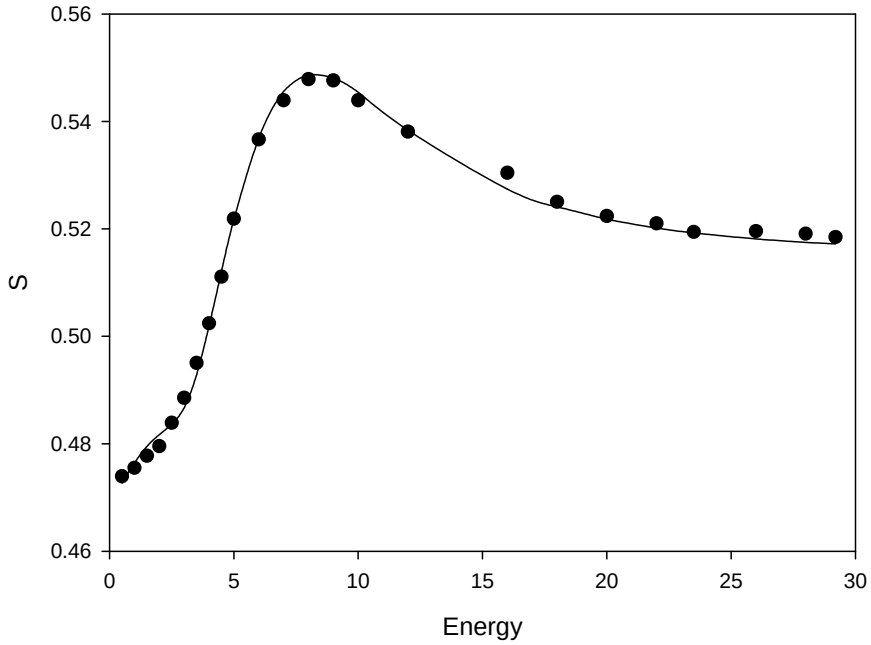

Figure 20 : S-Parameter against incident positron energy for sample P1.

Applying the Gaussian analysis technique, only a single type of defect was found which is assumed to be due to the V_{10} defect. A scaled *S*-parameter is also plotted to show the V_{10} peak already seen though *S-W* measurement.

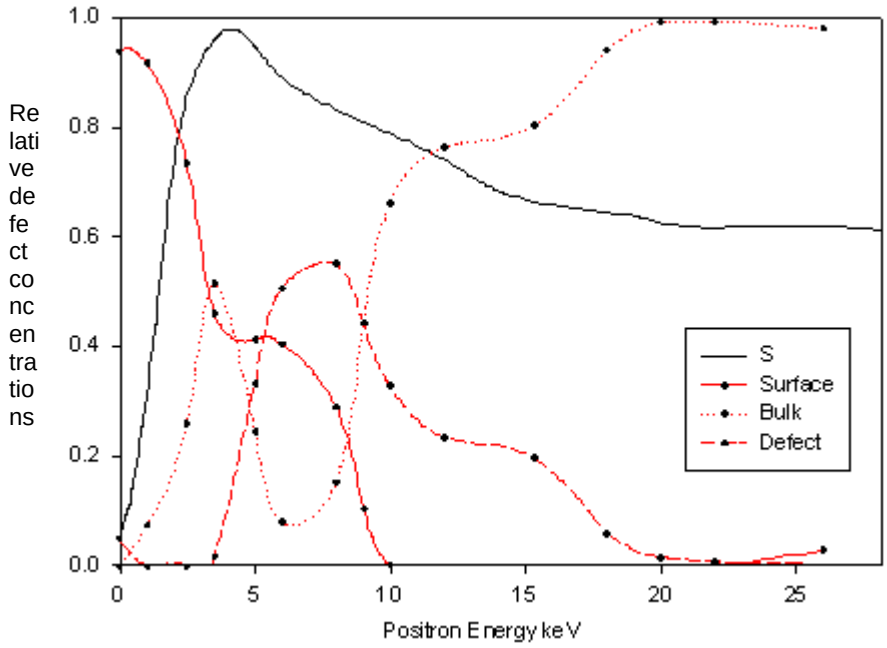

Figure 21 : Gaussian analysis derived defect concentrations for sample P1. Concentrations are relative with an arbitrary scale.

Figure 21 shows a three annihilation site Gaussian analysis of sample P1, fitting three Gaussian widths to collected positron annihilation data. Each characteristic Gaussian is attributed to a particular type of annihilation; the surface annihilations which are seen to become dominant at the surface of the material, the bulk which likewise dominates high energies, and a third component, which is labelled as a defect in the material.

The sample confirms the *VEPFIT* analysis (section 2.2.2) that shows the He-created defects to be concentrated in a buried layer. This is seen as the defect response in Fig 21 above. The defect does not appear at the surface and tails off with depth, a profile consistent with a band of defects below the surface. At shallower probe depths the sample appears as a virgin silicon sample, resulting in a rapid interchange of surface and bulk components as the positron energy is increased. This is abruptly halted as the defect layer is reached at 4-5keV positron energy. Just prior to the defect layer, a peaked surface-like component is seen that may be due to a buried oxygen layer

caused by the implantation process. It is known that implanting with an oxide layer on the sample will "knock" oxygen from the surface into bulk of the material. Under annealing the oxygen will become mobile and will tend to decorate the helium created voids. As the V_xO_y complex if far more stable than the V_xHe_y complex, the oxygen decoration would survive annealing. It is thought that due to the similarity between the buried oxide and the surface of the sample, the oxygen survives on the inner surface of the large void appearing as an internal, partially oxidised surface.

The third interesting feature is a flattened region of the bulk and defect components that occurs between 12 and 15keV positron energy. The response at this energy is reproducible and is not found in bulk silicon. It is believed that this corresponds to the bubble layer known to have formed in the sample. In this region the bubbles will appear as bulk silicon as positrons will become trapped on the clean surface. However it is also possible that a smaller number of V_{10} voids remain between the bubbles causing the observed bulk response.

The distribution of the voids and bubbles may be explained by looking at the implantation profile of the He using the SRIM-2003 modelling software [30], shown in Fig. 22. The size of features formed by annealing the implanted sample is a function of the concentration of helium initially present in the sample.

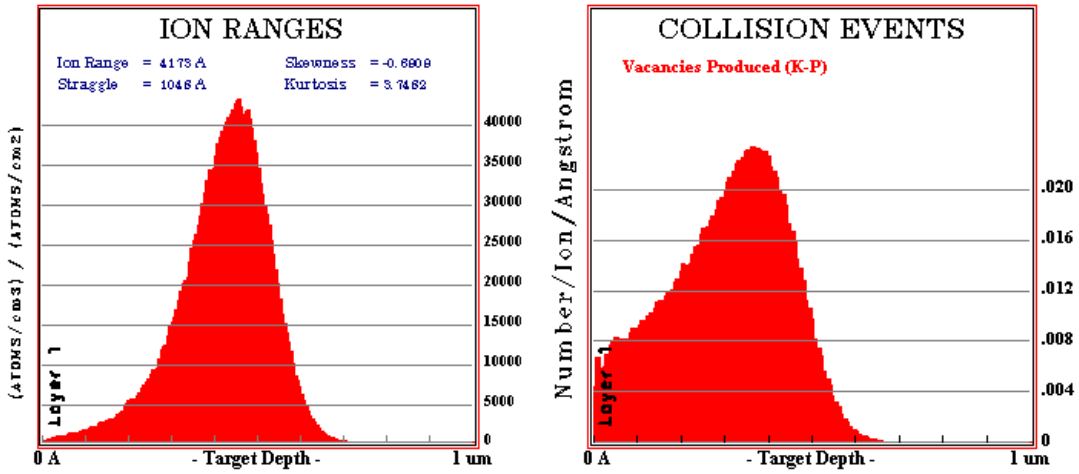

Figure 22 : SRIM simulations of helium ion implantation and damage profiles for sample P1. Right figure shows predicted vacancies caused by initial implant.

As should be expected the small voids are formed at the peak of the ion implantation. This would imply that the small voids are being formed between the larger bubbles in this region. This could be quite interesting if we assume that all of the positrons either get trapped on a surface of a bubble or in a void. This would give the ratio of void to bubble surface in the sample as there will only be trapping (or at least effective trapping at the surfaces of the defects).

This model does not support the theory of a bubble layer also containing some small voids at 1.5-2μm as all ions are found well before this. This is due to the temperature of implantation which is not included in SRIM calculations. Additional thermal energy allows greater depth diffusion of the helium, and increases the mobility of defect complexes subsequently formed.

All of the above work is consistent with the *S*-*W* analysis presented in prior sections, and it is assumed that the "defect" width is associated with V_{10} defects due to this analysis. However, this is circumstantial and must be confirmed by a combination of the two methods. Given that the total *S* parameter at any point may be expressed as a sum of fractional *S*; $S = S_1 f_1 + S_2 f_2 + ... + S_N f_N$. The experimental *S* can be compared with *S* constructed from the experimental values for $S_{surface}$ and S_{Bulk} and the previously determined defect value, and the Gaussian fractions; however, there is no correlation between the Gaussian derived fractions and the experimental data, as shown in Fig. 23 below.

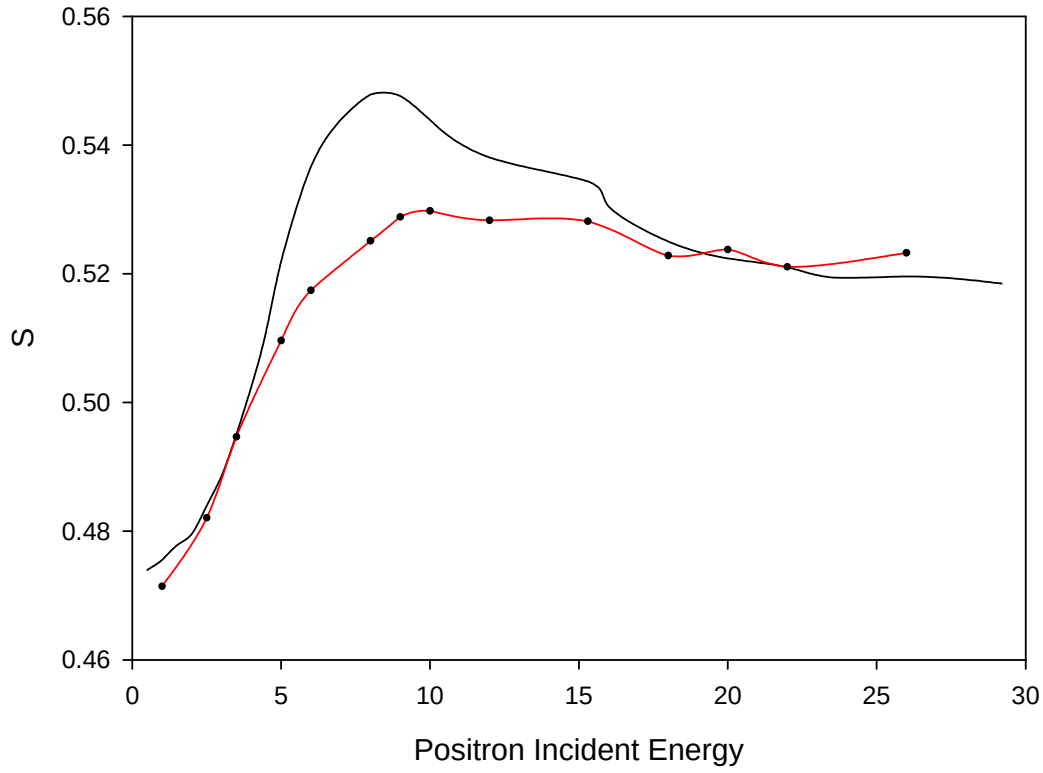

Figure 23: Comparison of experimental data for sample P1 (black line) and parameters calculated using known specific S parameters and Gaussian fractions (red line)

However, if the defect component S_{def} is fitted, a far superior fit may be achieved, as shown below in Fig. 24.

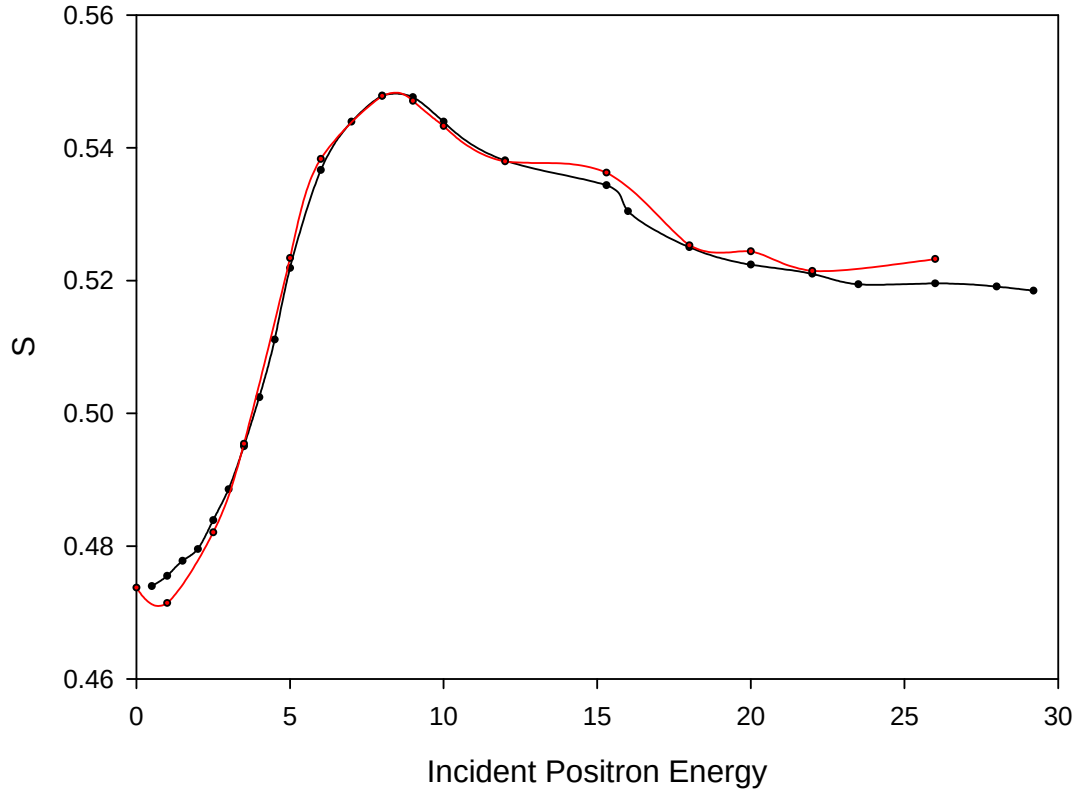

Figure 24: as for Fig. 23 but using a fitted defect S value

There is still some obvious discrepancies between the experimental data and fitted S_{def}, most noticeably at 15kV and towards the bulk. However the most important region of interest, the defect peak, is fitted well with an S_{def} of 1.161. As further confirmation of the approach the *S*-parameter of each Gaussian peak obtained using the analysis may be calculated and compared with the measured and fitted values.

S values	Experimental and fitted	Gaussian *S*
Bulk	1	1
Surface	0.909	0.912

Table 7 : Comparison of experimental and Gaussian derived S-parameters.

There is little difference between these two sets of values and throughout the defect layer the slightly increased Gaussian surface *S* may be compensated for by the lower bulk, producing a nearly identical fit with experimental data.

All this evidence now points to a conclusion different to that seen during *S*-*W* analysis and far more consistent with the electron microscope measurements taken by the University of Salford. The large *S*-parameter of the defect is in the saturation region of the S against void size extrapolation. Therefore no direct estimate of the defect size can be made, other than it is above 20 atoms in size as seen in Fig 7. This problem and an extension of the method to solve it will be further discussed in the following future work section. However it can be seen that a band of large bubbles decorated with a surface like state persists in the sample. The surface state is likely to be oxygen "knocked" into the sample during implantation and forming a V_xO_y complex at the internal surface of the bubbles.

As the defect layer of the silicon comprises two separate types of defects, the measured and fitted *S* is of a composition of the two. Thus a simple single defect box fit applied by VEPFIT would fail to spot the two different defects and report and S consistent with V_{10}-V_{12} defects as documented during the initial analysis.

Fitting the samples using the Gaussian analysis technique as described revealed two annihilation sites at the peak of the implantation damage (see Fig.25). The first corresponded to a larger defect than previously thought, certainly larger than 20 atoms in size, and likely at the maximum possible value for defects in silicon. Secondly a surface-like component was seen to exist at the same depth as the defect. It is believed that there is a silicon oxide complex of some form, most likely SiO_2, due to the similarity to the surface. The presence of this annihilation site accounts for the low measured *S*, which is taken as a superposition of the much higher defect *S* and the surface-like low *S* value.

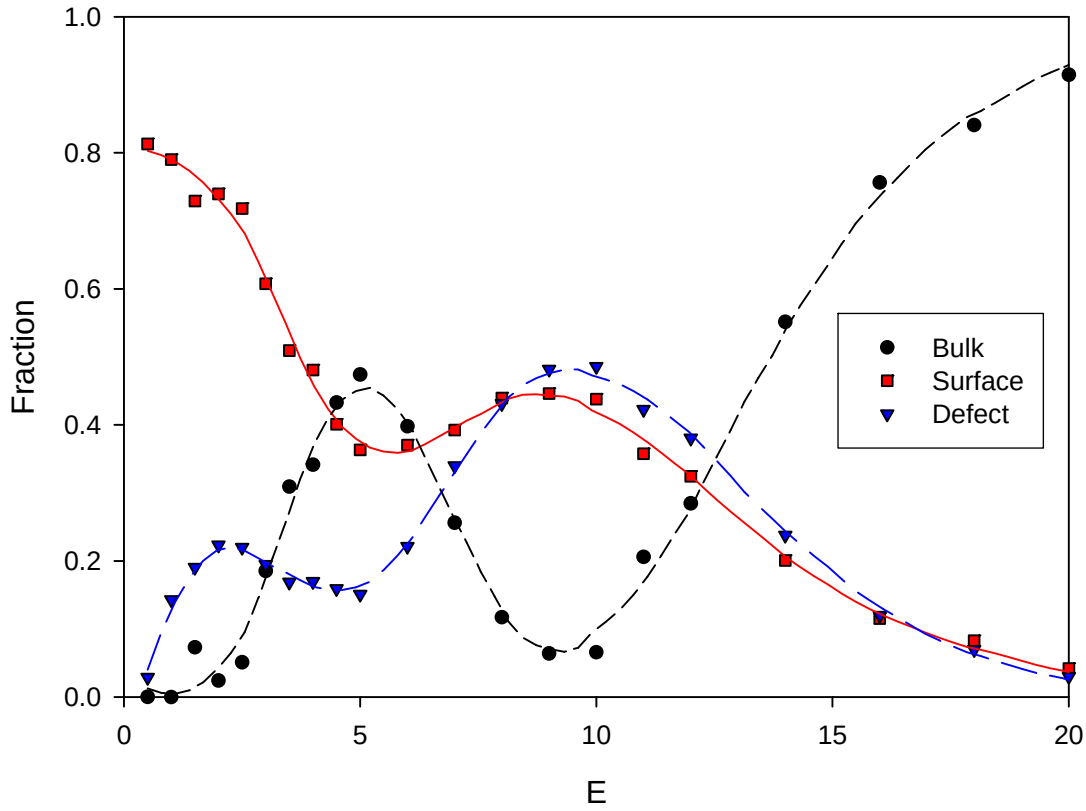

Figure 25. Gaussian analysis of He^+- created nanovoided silicon. Solid line and square points indicate surface-like state, short dash and circles show bulk contributions and long dash and triangles show defect sites with S = 1.20.

What was not known was the size of the defects measured, due to the lack of sensitivity in *S* at defects above 20 atoms in size. It was suspected that if sufficiently large, the interior surface of the defects would act as clear surfaces to the silicon during interaction. It is therefore necessary to check if clean internal surfaces may be detected by positrons, and if they cannot, how the internal surfaces of the voids under consideration here are not clean.

In order to observe any interaction at a possible clean *internal* surface the samples were heated to 700ºC to stimulate the formation of positronium in the defects. While it was observed that Ps was emitted from the external surface of the sample, there was no evidence, either by Gaussian analysis or direct examination of the gamma spectrum, of formation in the defect peaks. Therefore either the positrons are not trapping in large, nanometre sized defects or the defects themselves do not behave as clean internal

surfaces.

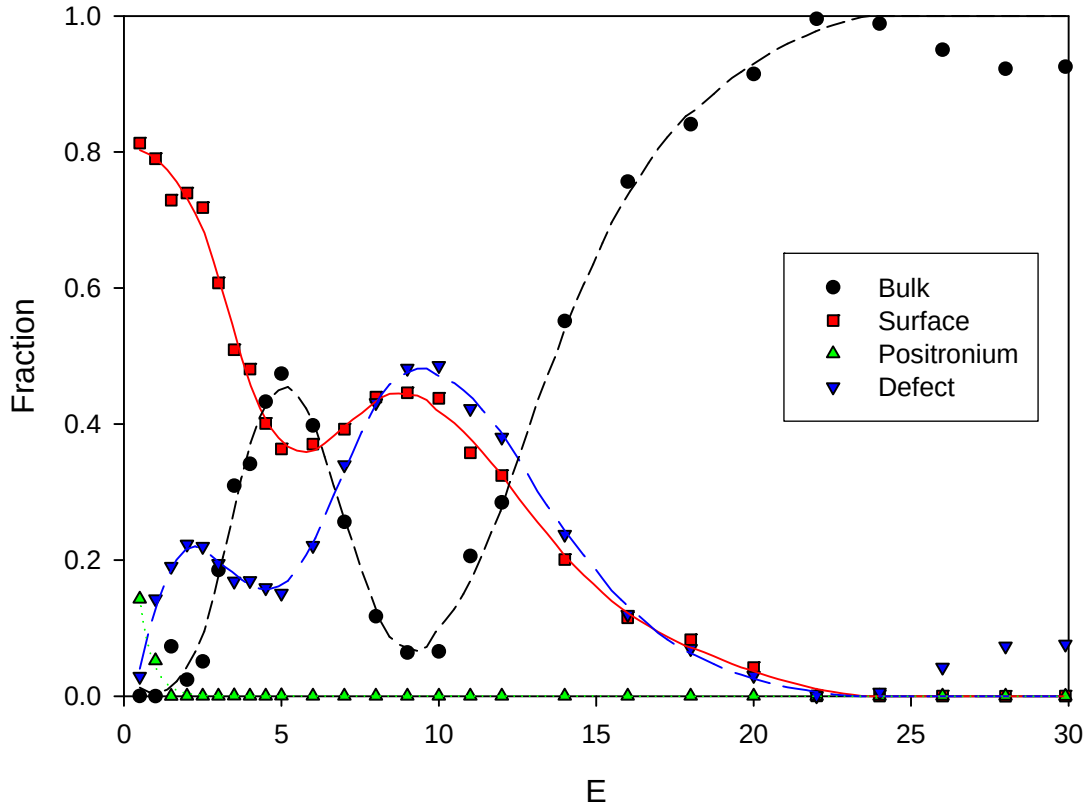

Figure 26. Gaussian analysis of nanovoided silicon at 700ºC, additional dotted component shows positronium formation at real surface only

The samples were annealed at 1100ºC for 15 minutes in order to remove any smaller vacancies. Following the anneal there was no evidence of the presence of large defects in the *S*-parameter or Gaussian analyses; however measurement by TEM continued to show well-defined nanovoids in a buried layer.

It is therefore proposed that positrons do not reach the nanovoids themselves, rather annihilating a possibly larger concentration of partial decorated smaller defects. It is also possible that the nanovoids simply do not trap the positrons at all or there is annihilation at their surface. However there is no evidence of a silicon bulk annihilation at the nanovoid layer and there is no evidence of surface phenomena such as positronium formation under heating.

It is not possible to calculate the size of the smaller defects, as they are above the limit

of size resolution of the technique. Two possible types of annihilation occur at these defects; the first is in an undecorated defect, the second most likely occurs at the oxygen decorated surface of a similar defect. The oxygen decoration appears the same as an oxide-coated external surface, with identical *S*-parameter. The oxygen most likely entered the sample during implantation of the hydrogen, which was performed in an insufficiently clean environment. These two annihilation sites trap all of the positrons that thermalise within a diffusion length of them, indicated by the lack of either positronium or bulk silicon signatures seen in the sample. The presence of either of these would indicate trapping in large voids or bulk, and there is no evidence of either.

3. FUTURE WORK

3.1 Polarised positron beam spectroscopy: introduction

In section 1.1.3 the fact that a slow positron beam can be highly spin-polarised was introduced. In this section pilot studies using the existing apparatus are described.

The measurements proposed use Doppler broadening of the annihilation radiation as a measure of the momentum distribution of the electrons at the annihilation sites. The principle underlying the application of spin-polarised positrons as a probe of magnetic structures is that positrons are ~1000 times more likely to annihilate an electron in the opposite spin state. Therefore, if the spin states of some of the electrons in a sample are changed (e.g. by measuring magnetic and non-magnetic samples, or by changing the external magnetic field direction), the difference in the Doppler broadening data yields information specifically on those electrons and thus the magnetic species. By using a controllable-energy positron beam semi-quantitative depth-dependent information can be obtained.

Rather than annihilating, it is also possible that positronium formation will hold spin information about the electron. As has been discussed elsewhere in this thesis, the formation of o-Ps to p-Ps in unordered materials is in a ratio of 3:1. As the formation is dependent on the relative spins of the positron and electron involved, it would be expected that introduction of ordered positrons (through the use of a helically polarised source) into a sample with ordered electrons, would produce a perturbation from this ratio. With an appropriate experimental set-up, it may be possible to detect this using lifetime measurements, peak-valley comparisons or Gaussian analysis spectrum fitting. While this is not attempted during the initial experiments documented in this section, and indeed it is unlikely that positronium would form at sufficient quantities in the polarised samples under consideration here, it should be considered for future work and expansion.

In order to best produce the two above situations, we desire a positron beam where the primary beta positron momentum may be selectively tuned such that in this case it is approximately parallel to the beam axis. It may be somewhat irrelevant the actual

direction of beam polarisation, as it should be straightforward to exam the null case (where an ordered beam is less likely to annihilate with spin polarised electrons). In the gross example studied below this is certainly the case as we are interested in comparison studies between the ordered and unordered states of a sample. It makes little difference whether we become more or less sensitive to the polarised electrons in this case. As it is intended that a polarised positron would be used as a 'magic bullet' to selectively probe spin sensitive clusters or defects, then selection of the spin direction would be a useful extension to the work, however it is currently unnecessary.

The problem with 'standard' laboratory-based positron beam systems such as that employed in this study is that, in order to maximise the positron beam intensity, (a) the radioactive source is deposited on a high-Z backing to maximise backscattering and hence the forward-going flux, and (b) the moderator – in our case an annealed tungsten mesh – is placed as close as possible to the source to maximise the solid angle of irradiation. Both (a) and (b) increase significantly the effective spread of emission angles of the beta positrons which contribute to the final slow positron beam, and this spread consequently reduces the beam polarisation in the axial direction of implantation into a sample. (a) and (b) will be overcome, as discussed below.

The spin polarisation of a positron beam is given by [34]

$$P = (v/2c)(1+\cos\alpha) \qquad \text{- (6)}$$

where v is the emission velocity, c the speed of light, and α the half-angle of the cone of acceptance of beta positrons at the moderator. (v/c is called the helicity.) For positrons emitted in a cone of half-angle 30º from the commonly-used source ^{22}Na, $P \sim$ 70%. Other sources with higher helicity have shorter half-lives; for example, if ^{68}Ge were to be used instead of ^{22}Na then $P \sim 94\%$, but its half life of 271 days would make it an impractical choice, and its higher end-point energy would additionally make the moderation process less efficient.

Depolarisation of the positron beam upon thermalisation in the moderator depends on the incident energy and, as the highest-energy positrons from the decay of ^{22}Na have ~ 540 keV, an average depolarisation of only a few percent is expected. The subsequent depolarisation of the implanted mono-energetic positrons (maximum energy ~ 30keV) is also expected to be small.

3.2 Pilot measurements

Three samples were used in initial measurements; high purity iron, single crystal silicon and annealed copper. The samples were measured with and without a fixed magnet of approximately 0.75T placed behind the sample, and aligned to accelerate positrons into the sample. It was assumed that the magnet would be sufficiently powerful to align the majority of susceptible electrons in each sample, thus presenting a highly ordered and polarised material to study. Measuring with and without the magnet allowed for comparisons between the ordered and unordered states to be made. Where possible two measurements were made concurrently, at low and high positron implantation energies. This allowed sampling of the electron spin state in both surface and bulk states.

The iron sample was annealed to above the Curie temperature of iron between measurements. This removed any remnant of order in the sample which could have remained after exposure to the intense magnetic field. It should be noted that the magnetic confinement of the positron beam may cause the sample to retain some order without the addition of the permanent magnet. While there was no obvious signs of this when checking with a Gauss probe, as with many aspects of these trial measurements, further consideration may be required in future work.

In order to increase the helicity of the beam the positron source was placed 25mm away from the tungsten moderator, reducing the solid angle available to the generated positrons and thus reducing the range of possible spin polarisations (equation (6)). As discussed above. This reduced the count rate to below 10^2 s^{-1}, requiring long run times of several hours to produce statistically favourable results. Unfortunately, the increased running time left the measurements vulnerable to systematic drift and shifts, and required careful (and non-uniform) background subtraction.

In trial measurements with the current Bath positron beam a piece of annealed high-purity iron was used as the target, with and without a rare earth magnet placed behind it (local field ~ 0.75T). In the second case the sample was annealed to above its Curie temperature. The source was placed 25mm from the tungsten moderator in an attempt

to reduce the depolarisation effects of backscattered positrons and a large range of emission angles. The annihilation lines were recorded in the two cases and the ratio is presented in Fig.27.

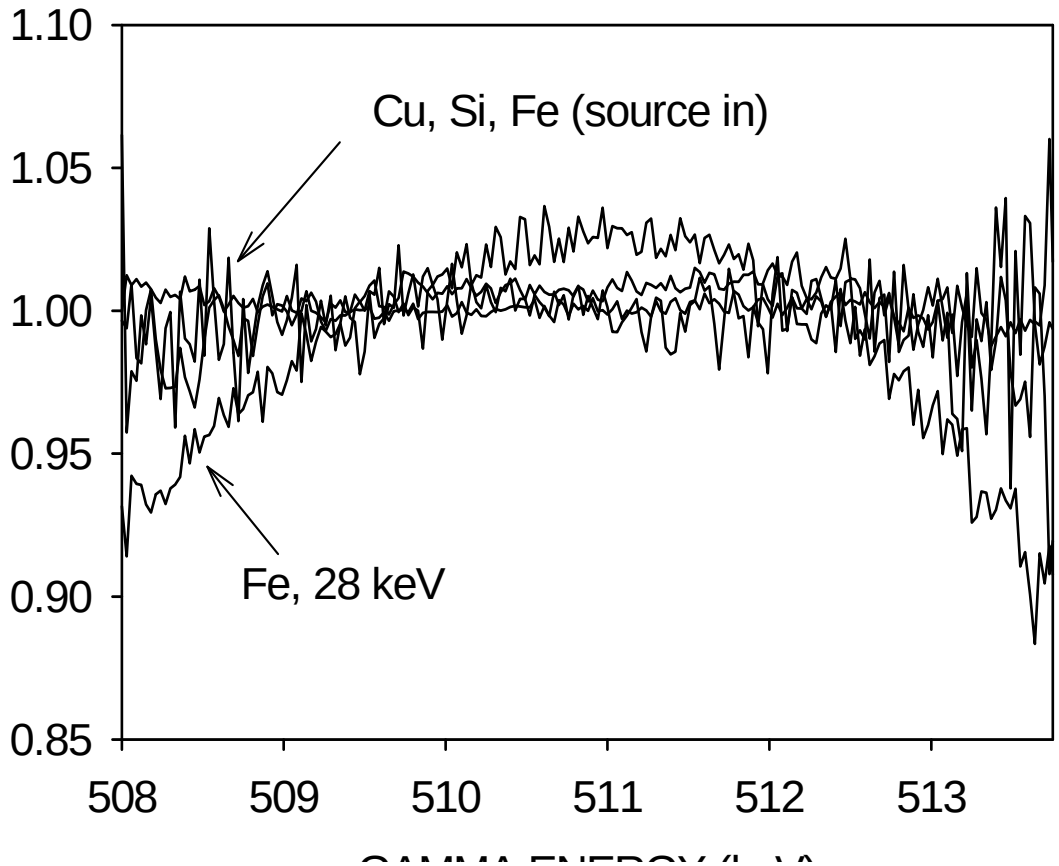

Figure 27: Ratios of annihilation gamma ray energy spectra (centred at 511keV) with and without a 0.75T field at the sample position: beam energy 28keV (depth ~ 2 μm). Data showing constant ratio of 1.0 are for Si, annealed Cu, and Fe with the source adjacent to the moderator mesh (ie 'usual' position).

To check for systematic influences on the spectra the same measurements were made for single-crystal silicon and for annealed copper samples. The clear difference between iron and silicon and copper, which both gave null results, is seen in the figure. In magnetically-saturated iron the 3d electrons are polarised in the magnetisation direction; their momentum distribution is relatively broad and, if their spins are antiparallel to that of the incident positrons, the annihilation line is Doppler broadened, and vice-versa. The pilot results show that the latter situation holds here – i.e., fewer positrons annihilate the 3d electrons when the magnet is in place.

The positive result of the pilot measurements is an indication of the potential of a polarised positron beam annihilation spectrometer, but the current beam is impractical principally because (a) the positron count rate was reduced to below 10^2 s^{-1}, requiring very long runs with the possibility of unwelcome drifts and instabilities affecting the data, and requiring careful background subtraction, and (b) the beam polarisation was not optimised (note that a null result was also obtained for Fe when the source was held in its usual position with respect to the moderator). It should be remembered also that the changes seen in the figure are the largest that might normally be expected to be measured; small changes resulting from, for example, a low concentration of magnetic species, require significantly better statistics and good stability.

The development of novel materials containing magnetic nanoparticles and magnetic semiconductor layers for spintronics applications suggests that the time for this technique to be implemented has come.

4. SUMMARY

There has been considerable advancement in the understanding of nano-voids in Silicon, with the presentation of evidence that positrons in fact fail to find the large voids. Instead they trap in a previously unknown layer of much smaller vacancies. In the samples studied these were partially decorated with oxygen, although it is presumed that implantation in a different atmosphere would produce alternative decorations.

It has been shown that the superposition of these two states (small undecorated vacancy and small decorated vacancy) in fact produce the S-parameter of 1.12 seen in literature. This is at odds to work presuming that either large nano-voids show this signature, or that two different sizes of vacancy cause this value of S.

It has been shown that a sample annealed so that it will only contain nano-voids has no measurable positron response over bulk silicon. Whether this is a question of effective cross-section, an inability for the positron to trap in the nano-void, or immediate pickoff at the voids clear internal surface, is a question for future research.

Of more immediate concern for users of nano-voided silicon is the formation of the smaller defects. Under annealing these do become mobile and are eventually removed, but the trapped complexes are of interest. While in the case studied here they were unwanted impurities, they may in fact be a useful tool to direct implanted ions to areas and depths of interest. This is of course one of the reasons for research in nano-voided materials.

The sensitivity of positrons to the smaller defects shows an important use of the technique as the more conventional SEM and TEM measurements were unable to detect them. The use of Gaussian fitting allowed classification of the defects, the percentage of ion complexes, and the type of complex itself. Extension of the technique can hopefully be used in any number of future systems to study ion complexes.

Also presented was preliminary work on spin polarised samples. While much of this

resurrects a decades old technique, there have been very few positron studies of spin. With the increasing interest in spintronics and spin designed materials, it is hoped that the positron will be an effective measure in their future development.

REFERENCES

1 – Dirac, P.A.M., "A theory of electrons and protons", Proc. Roy. Soc. London A, 126 360-365 (1930)
2 – Weyl, H.K.H and others, (1930)
3 – Anderson, C.D., "The positive electron", Phys. Rev., 43 491-494 (1932)
4 – Blackett, P.M.S., Occhialini, G.P.S., "Some photographs of the tracks of penetrating radiation", Proc. Roy. Soc. London A, 139 699-718 (1933)
5 – White, M., Lessner, E., "Slow positron target concepts for the advanced photon source (APS) linear accelerator", Positron Annihilation Materials Science Forum 255 778-780 (1997)
6 – Yang, B.L, et al, "The slow positron beam based on Beijing electron-positron collider", Positron Annilihation, ICPA-13, Proc. Mat. Sci. Forum 445 513-515 2004
7 – Gribbin, J., "Q is for Quantum", Weidenfeld & Nicolson (1998)
8 – ed. Coleman, P., "Positron beams and their applications", World Scientific Publishing (2000)
9 – Charlton, M., Humberston, J.W., "Positron Physics", Cambridge University Press (2001)
10 – Ore, A., Powel, J.L., "Three photon annihilation of an electron-positron pair", Phys. Rev. 75 1696-1699 (1949)
11 – Adachi, S., Chiba, M., Hirose, T., Nagayama, S., Nakamitsu, Y., Sato, T., Yamada, T., "Precise measurements of e+e- annihilation at rest into four photons and the search for exotic particles", Phys. Rev. A 49 3201-3208 (1994)
12 - J. Störmer, A Goodyear, W Anwand, G Brauer, P G Coleman and W Triftshäuser J. Phys.: Condens. Matter 8 L89-94 (1996)
13 - P.W. Zitzewitz, J.C. Van House, A. Rich and D.W. Gidley, Phys. Rev. Lett. 43, 1281 (1979).
14 – Ruark, A.E., "Positronium", Phys. Rev. 68 278 (1945)
15 – Yang, C.N., "Selection rules for the dematerialisation of a particle into two photons", Phys. Rev. 77 242-245 (1950)
16 – Y., Murakami, H., Kinoshita, A., "Positron Annihilation in Porous Silicon", App. Phys. Lett. 63 2798-2799 (1993)
17 – Brusa RS, Macchi C, Mariazzi S, et al, "Absence of positronium formation in clean buried nanocavities in p-type silicon", Phys. Rev. B 71 Article No. 245320 (2005)
18 - Costello, D.G., Groce,D.E., Herring, D.F., and McGowan, J.Wm., 1972, *Phys Rev* B 5, 1433.
19 - Canter, K.F., Coleman, P.G., Griffith, T.C. and Heyland, G.R., 1972, *J Phys* B 5, L167.
20 - L.D. Hulett, Jr., J.M. Dale and S. Pendyala, 1984, *Mat. Sci. Forum* 2, 133.
21 - C.D. Beling, R.I. Simpson, M. Charlton, F.M. Jacobsen, T.C. Griffith, P. Moriarty and S. Fung, 1987, *Appl. Physics* A, 42, 111.
22 – Hakala, M., Puska, M.J., Nieminen, R.M., "Momentum distributions of electron-positron pairs annihilating at vacancy clusters in Si" Phys. Rev. B, 57 (13) 7621-76271 (1998)
23 - 16 – Parisini, A., Angelucci, R., Dori, L., Poggi, A., Maccagnani, P., Cardinali, G.C., Amato, G., Lerondel, G., Midellino, D., "TEM characterisation of porous silicon", Micron 31 223-230 (2000)
24 – Lamedica, G., Balucani, M., Ferrari, A., Bondarenko, V., Yakovtseva, V., Dolgyi,

L., “Gettering technology based on porous silicon”, Solid State Phenomena 82-84 405-410 (2002)
25 – Piatkowska, A., Gawlik, G., Jagielski, J., “AFM studies of hydrogen implanted silicon” Applied surface science 141 (1999) and M. Bruel, European Patent No. 0 533 551 A1, 1992
26 - Föll, H., Christopherson, M., Carstensen, J., Haase, G., Formation and application of porous silicon. *Mater. Sci. Eng.* 39, 93–141. (2002)
27 – Raineri, V., Saggio, M., Rimini, E., “Voids in silicon from He implantation: from basic to applications”, J. Mater. Res. 15 1449-1477 (2000)
28 – Brusa, R.S., Karwasz, G.P., Tingo, N., Zecca, A., Corni, F., Calzolari, G., Nobili, C., J. App. Phys. 87 2390 (1999)
29 – H. Moriceau, J. Elec. Mat. 32 892 (2003)
30 - Ziegler, J.F., Biersack, J.P., Littmark, U., “The Stopping and Range of Ions in Solids”, Pergamon Press, New York (1985)
31 – McKenzie, I., Phys Lett. 30 115-116 (1969)
32 – Van Veen, A., Schut, H., de Vries, J., Hakvoort R.A., Ijpma, M.R., “Analysis of positron profiling data by means of VEPFIT”, Positron Beams for Solid and Surfaces 218, AIP Conference Proceedings 171-196 (1990)
33 - J. Major, in *Positron Beams and their Applications*, ed. PG Coleman (World Scientific, 2000) p 259.
34- Staab, T.E.M., Sieck, A., Haugk, M., Pusta, M.J., Frauenheim, T.A., Leipner, H.S., Phys. Rev. B, 65 115-120 (2002)